Role of Lamin A and Lamin B2 in chromosome positioning in the interphase nucleus

A thesis submitted towards partial fulfillment of

BS MS Dual Degree programme

By

Suryesh Kumar Namdeo

Under the guidance of

Dr. Kundan Sengupta

(Assistant Professor, IISER Pune & Wellcome-Trust DBT India Alliance Intermediate Fellow)

Chromosome Biology Lab

Indian Institute of Science Education and Research

Pune

Certificate

This is to certify that this dissertation entitled "**Role of Lamin A and Lamin B2 in chromosome positioning in the interphase nucleus**" towards the partial fulfillment of the BS-MS duel degree programme at the Indian Institute of Science Education and Research (IISER) Pune, represents original research carried out by Suryesh Kumar Namdeo at CHROMOSOME BIOLOGY LAB (CBL), IISER Pune under the supervision of Dr. Kundan Sengupta, Assistant Professor, IISER Pune during the academic year 2013-2014.

Name and Signature of the student

Suryesh Kumar Namdeo

(Kundan Sengupta)

Supervisor

Date:

Place:

Head (Biological sciences)

Date:

Place:

Declaration

I hereby declare that the matter embodied in the report entitled "**Role of Lamin A and Lamin B2 in chromosome positioning in the interphase nucleus**" are the results of the investigations carried out by me at the Department of Biology, Indian Institute of Science Education and Research (IISER) Pune, under the supervision of Dr. Kundan Sengupta, Assistant Professor, IISER Pune and the same has not been submitted elsewhere for any other degree.

Name and Signature of the student

Suryesh Kumar Namdeo

Date:

Place:

Acknowledgement

I express my deep sense of gratitude to Dr. Kundan Sengupta, Assistant Professor, Chromosome Biology Lab, Indian Institute of Science Education and Research Pune who was kind enough to provide me an opportunity to explore various domains of scientific research during my course program. I am grateful to IISER Pune for providing all the research facilities and support they provided during this project.

I express my sincere gratitude to all lab members Devika, Ayantika, Roopali, Shivsmriti, Apoorva, Maithilee and Ajay for their valuable guidance, constant encouragement, immense patience and cooperation throughout my project work.

I am eternally grateful to my family. I am here because of blessing of my ever loving parents.

Suryesh Kumar Namdeo

Abstract

Lamins are the scaffolding proteins and major components of nuclear lamina present at the inner nuclear membrane and chromatin and provide mechanical and structural integrity to the nucleus. In addition, Lamins are also involved in a number of other fundamental cellular processes including DNA replication, DNA damage response, epigenetic regulation and mechanotransduction. These proteins have been reported to interact with specific regions of the genome known as Lamin associated domains (LADs). In this study we employed siRNA-mediated gene silencing approach to knockdown Lamin A and Lamin B2 genes in HEK293 cells. Our study demonstrates that depletion of Lamin B2 causes significant alteration in intranuclear positioning of peripheral chromosome 18 and inactive X (Xi) chromosome territories whereas no significant alteration was observed in positioning of the more centrally located chromosome 19 territory upon depletion of Lamin A and Lamin B2. Chromosome territories exhibit changes in their volume and surface area which signifies large scale topological changes upon Lamin B2 depletion. Expression status of candidate genes on X chromosome was lowered upon Lamin B2 knockdown. Taken together, these studies suggest a more prominent role of Lamin B2 compared to Lamin A in maintaining subnuclear positioning of peripheral chromosomes.

List of Figures and tables:

CHAPTER 1

INTRODUCTION

The nucleus is the most prominent organelle present in eukaryotic cells. It contains chromatin and various nuclear bodies such as nucleolus, cajal body, PML bodies and nuclear speckles (Figure 1.1). Each of these non-membrane structures within the nucleus has distinct functions but also physically interact with chromatin domains. Chromatin can be generally classified as either heterochromatin or euchromatin where heterochromatin is largely transcriptionally repressed and euchromatin is transcriptionally active region of the genome. Heterochromatin displays preferential localization either towards the nuclear periphery or perinucleolar regions, while euchromatin is transcriptionally active and has a more internal localization (Solovei et al., 2013).

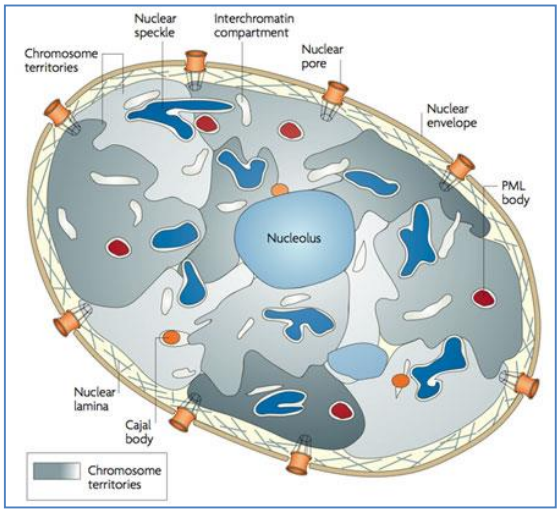

Figure 1.1: Organization of cell nucleus in higher vertebrates (Adapted from Lanctot et al., 2007)

The nuclear envelop is composed of inner nuclear membrane (INM) and an outer nuclear membrane (ONM), separated by ~30–50 nm (Figure 1.2). The inner nuclear membrane (INM) has intermediate filaments beneath them which form the nuclear lamina. Some of the functionally most important are Lamin family proteins, which are type V intermediate filament proteins (Dechat et al., 2008). Lamins are highly evolutionarily conserved as they are present in all metazoans (Melcer et al., 2007). Lamins are classified in two categories: A type lamins and B type lamins based on their sequence, structure and biophysical properties. A type lamins (Lamin A & C)

are encoded in *LMNA* gene and are the product of alternate splicing (Dittmer and Misteli 2011; Bokenkamp et al. 2011). B type lamins (Lamin B1 & B2) are encoded by *LMNB1* and *LMNB2* (Dittmer and Misteli 2011; Schumacher et al. 2006). Lamins apart from being a structural protein which tethers the chromatin have been reported to be involved in cellular processes such as mechanotransduction, transcription, DNA damage response, replication, development and epigenetic regulation (Dechat et al. 2008; Dittmer et al., 2011; Simon et al., 2011). Mechanisms behind most of these processes remain largely obscure. Mutations in lamins lead to a variety of disorders which are collectively termed as laminopathies (Worman, 2012; Butin-Israeli et al. 2012).

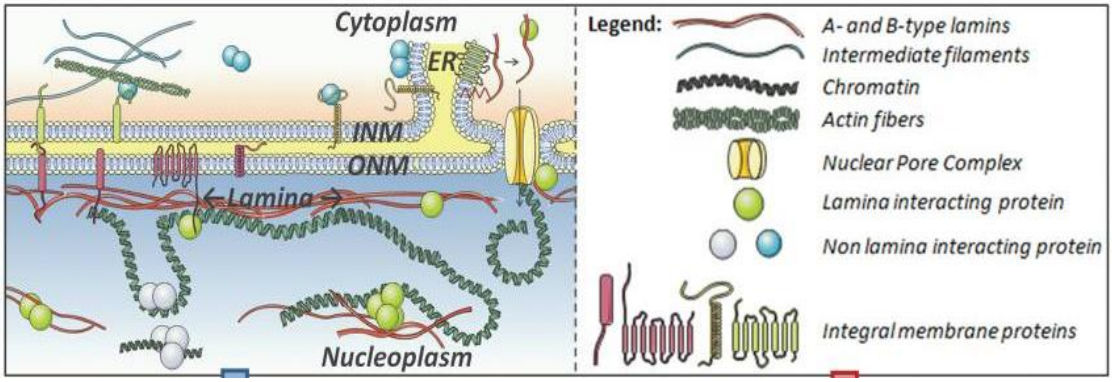

Figure 1.2: Organization of Lamins inside the nucleus (Adapted from Kubben et al, 2010)

Lamins interact with chromatin directly and specific genomic regions of Lamin interaction are referred to as Lamin associated domains (LADs) (Guelen et al., 2008). LADs are considered to be repressive as they consist of low gene density regions and genes which show low expression levels. Repressive epigenetic marks such as DNA methylation, H3K27me3, H3K9me2 and deacytylated histones are also abundant in LADs (Guelen et al., 2008, Prokocimer et al., 2009). LADs are generally conserved across multiple cell lineages with some small scale alteration during differentiation (Peric-Hupkes et al., 2010). One recent study reveals displacement of chromosome 13 in *LMNA* mutant fibroblast (Mewborn et al., 2010). This study also reveals no significant alteration in chromosome 7 which suggests that chromosomal mislocalization is not a general effect of *LMNA* mutant or null cells and the phenotype could be specific to certain chromosomes. Lamins have been proposed to act as anchors in facilitating heterochromatin organization in proximity to the nuclear membrane (Figure 1.3).

Spatial organization of DNA in interphase nucleus is non-random. Chromosomes are organized as individual chromosome territories in the interphase nucleus occupying a distinct sub-volume in the interphase nucleus. In general, gene rich chromosomes are closer to the nuclear center, while gene poor chromosomes exhibit more peripheral localization within the nucleus (Croft et al. 1999; Bolzer et al. 2005). Chromosome territories exhibit a probabilistic mode of spatial organization with differential interaction frequencies with each other (Lieberman-Aiden et al., 2009). This also results in segregation of active and inactive chromatin in nuclear space (Simonis et al., 2006; Lieberman-Aiden et al., 2009) which suggests that transcriptional activity being a very important player in determining three dimensional organization of nucleus. Spatially segregated chromatin regions also tend to diverge in their epigenetic marks, for example active and inactive chromatin regions have very different epigenetic marks (reviewed in Heard, 2005). These epigenetic marks such as DNA methylation and histone modifications may be required in determining three dimensional chromatin conformations (Matarazzo et al., 2007; Calabrese et al., 2013). One unique example of a correlation between distinct epigenetic marks and spatial organization is the mammalian female inactive X chromosome (Xi). Active and inactive X chromosomes in females are genetically homologous but are different in terms of epigenetic marks and spatial organization (Clemson et al., 2006, Heard, 2005). Inactive X chromosome or Barr bodies are localized towards the nuclear periphery (Barr et al., 1949, Heard, 2005).

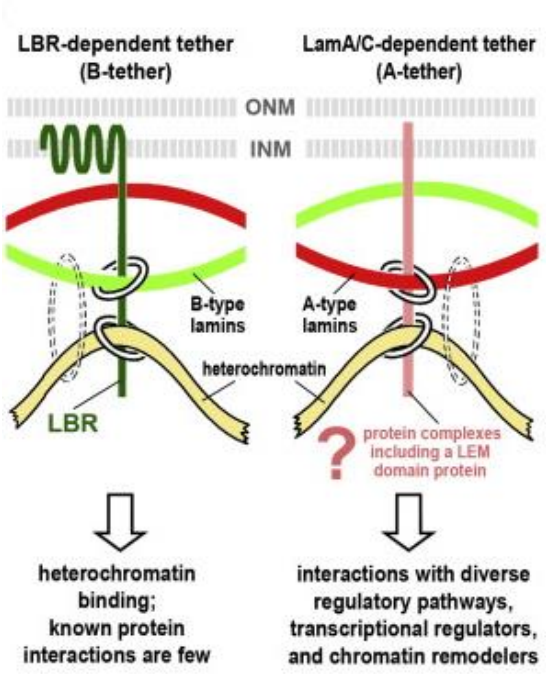

Figure 1.3: Proposed model of heterochromatin organization in proximity of nuclear membrane. (Adapted from Solovei et al., 2013). LBR: Lamin B receptor.

X chromosome inactivation (XCI) is a process to transcriptionally silence one of two X chromosome in females to achieve dosage compensation between males and females (Gendrel et al., 2011). XCI occurs during early embryonic development and

leads to random transcriptional inactivation of one of the X chromosomes. XCI begins with transcription of XIST long non coding RNA from one of the X chromosomes during embryonic stage. XIST transcript accumulates along cis X chromosomes and recruits polycomb repressive complexes (PRC1 and PRC2). An alteration in the epigenetic state of chromatin accompanies a decrease in active chromatin marks such as acetylated histones; and spread of repressive marks H3K27me3, H4K20me1 and DNA hypermethylation on promoter sequences (Figure 1.4). This is followed with the incorporation of histone variant macroH2a which ultimately leads to transcriptionally silent late replicating chromatin (reviewed in Wutz, 2011). However, some genes escape this inactivation process and remain transcriptionally active in Xi. These genes usually have their homologs present in male Y chromosome and hence do not require dosage compensation between sexes. These genes are located in pseudoautosomal region (PAR) of X chromosome and may form active chromatin loops or are present at the edge of inactive X chromosome (Xi) territory (Chaumeil et al., 2006).

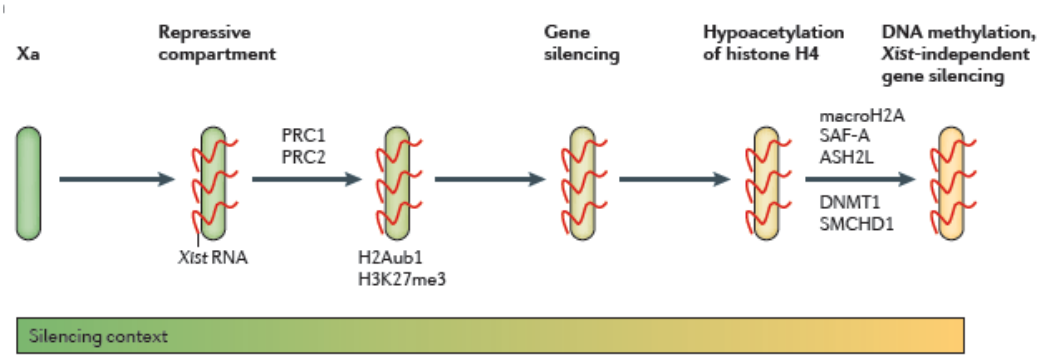

Figure 1.4: Sequence of accumulation of different Xi specific modification during X chromosome inactivation. (Adapted from Wutz, 2011)

In order to discriminate active and inactive X chromosomes different Xi specific marks such as H3K27me3, macro H2A and XIST RNA coating can be utilized. Decrease in H3K27me3 levels in Lamin A mutant cells have been reported previously (Shumaker et al., 2006; Hakelien et al., 2008). Depletion of Lamin B1 in senescent cells exhibit global changes in H3K27me3 distribution (Shah et al., 2013). However, whether this alteration in H3K27me3 levels also correlates with Xi chromosome positioning still remains elusive.

The primary aim of this study is to examine the role of Lamin A and Lamin B2 in the positioning of X chromosome territories in the interphase nucleus. This was performed by siRNA mediated knockdown of Lamin A and Lamin B2 followed by 3D FISH for X chromosome territory or macro H2A immunostaining for inactive X (Xi) territory localization. Gene expression levels of candidate genes present on X chromosome was also examined in Lamin A and Lamin B2 depleted cells in order to examine the role of lamins in their expression. Genomic loci FISH was performed on candidate genes so as to assess the effect of lamin depletion in their positioning within the X chromosome territory.

CHAPTER 2

MATERIALS AND METHODS

1. Cell culture: HEK293 Human embryonic kidney cells, MCF7 Human breast cancer cells, SW480 human colorectal cancer cells and WI-38 Human primary lung fibroblast cells were grown at 37°C in the presence of 5% CO_2 in DMEM media supplemented with Penicillin (100 units/ml)/Streptomycin (100 µg/ml) and 10% heat inactivated filtered FBS.

2. Cell fixation and permeabilization: Cells were grown on cover slips overnight. Cells were washed 2 times in 1X PBS (last wash on ice), 5 min each. Cold Cytoskeletal (CSK) buffer treatment was given for 4min, fixed in 4% freshly prepared PFA (pH 7.4) for 10min. Cells were then washed with 0.1M Tris-Cl (pH 7.4) for 10 min followed by 1X PBS washes 2 times for 5 min each. Cells were permeabilized with 1ml of 0.5% of Triton-X-100 prepared in 1X PBS for 10 min at RT. Following permeabilization, cells were incubated in 20% glycerol for 60 min and were subjected to four freeze thaw cycles in liquid N_2. Cells were washed in 3 times 1X PBS wash for 5 min each. Cells were then treated in 0.1N HCl for 10 min at RT. They were washed 3 times in 1X PBS and then stored in 50% Formamide/2XSSC mixture (pH 7.4) at 4°C.

3. Indirect Immunofluorescence assay: Immunofluorescence was performed by modifying the protocol described in Calle et al (2008) for nucleolar proteins [31]. Cells were blocked in blocking buffer (1% BSA + 0.5% Tween 20 in PBS) for 1 hr. Cells were treated with primary antibodies [Rabbit polyclonal anti macroH2A, 1:500 (Abcam), mouse polyclonal anti Lamin A, 1:50 (Epitomics, Jol2 antibody), mouse monoclonal anti B2, 1:500 (Abcam)] and incubated at RT for 2 hrs. Two 1X PBS washes were given and one 0.1% Triton–X-100 in 1X PBS for 5 min each. Cells were incubated with secondary antibody (Alexa fluor 568 goat anti mouse and/or Goat anti rabbit-FITC) for 45 minutes at RT. Cells were washed in 1X PBST for 5 min each and counterstained with 0.04% DAPI for 3 min. One wash of 1X PBS for 2

min was given and then cells were mounted in Antifade mounting medium (Invitrogen) and stored at 4℃, until they were imaged.

4. Metaphase preparation and DAPI staining: 0.4 X 10^6 cells were seeded in a T-25 flask. After 12-16 hours, cells were treated with 1% colcemid for 90 minutes at 37°C. The media (with colcemid) was collected in a tube. Cells were washed with DPBS. Cells were trypsinized with 750 µl trypsin for 3 minutes at 37°C, 1500 µl of media was added to the flask. Cells, media and DPBS were collected in the same tube. Cells were then centrifuged at 1200 rpm for 10 minutes at 10°C. To the pellet, 5 ml pre-warmed 0.075 M KCl was added drop wise and incubated at 37°C for 30 minutes to allow cell swelling. The reaction was terminated by adding few drops of fixative (3:1 Methanol to Glacial acetic acid) and centrifuged again to obtain the cell pellet. To the pellet 8 ml of fixative was added and centrifuged. The pellet was mixed with 100-120 µl of fixative and dropped on clean glass slides. Metaphases were then treated with ethanol series (70%, 90% and 100%) to dehydrate the DNA. The metaphases were then stained with DAPI for 3-5 minutes and washed in 2X SSC buffer. Slides were mounted with antifade and imaged using a fluorescense microscope (Zeiss) under a 63X oil objective (N.A = 1.4).

5. 3D-Fluorescence in situ hybridization (3D-FISH): FISH hybridization was performed using whole chromosome paints (WCP) from Applied Spectral Imaging for chromosomes X, 18 and 19. 2µl probe per chromosome per coverslip and 1µl of Human Cot-1 DNA probe per coverslip was used for these experiments. Probes were vortexed at 37°C for 5 min at 500-800 rpm and denatured at 80°C for 5 min. Probes were quick-chilled on ice for 2 min, followed by pre-annealing for 45 min at 37°C. 5 µl probe was applied on a coverslip. Co-denaturation of genomic DNA and probes was performed at 80°C for 5min. Slide was left for hybridization in 37°C incubator for 48 hours.

FISH detection: Slides were washed with 50%Formamide/2XSSC, 3 times at 45°C followed by 0.1XSSC washes 3 times at 60°C. Coverslips were briefly treated with 4X SSC/0.1% Triton-X-100 and counterstained with DAPI for 2 min. Slides were washed with 2X SSC for 5 mins and mounted with Antifade and stored at 4°C.

6. Metaphase Fluorescence in situ hybridization: Probe pre-annealing is identical as described in 3D FISH experiment above. 5 µl of total probe mix per slide was

used. 50 µl of 50% Formamide/2XSSC (pH=7.4) was added on metaphases and then they were denatured at 80°C for 1min. Metaphases were then treated with 70% ice cold ethanol, 90% ethanol and 100% ethanol; 1min for each treatment. Metaphases were then allowed to air-dry completely. 5 µl of pre-annealed probes were then added on metaphase containing region of slide. A 22 x 22 coverslip was mounted on this region and the coverslip was sealed with nail-polish and hybridized at 37°C for 48 hours. Metaphase FISH detection protocol is similar to as described for 3D FISH washes with only difference of washes being performed on slides instead of coverslips.

7. Imaging and analysis: Confocal images of fluorescently labeled (chromosome paints, secondary antibodies and gene specific probes) DLD1 cells were acquired in a LSM710 Zeiss Laser Scanning system at a constant voxel size of X=Y=0.105µm, Z=0.35µm under a 63X, Numerical Aperture = 1.4, oil objective. Each image was an 8-bit, 512X512 image, at constant scan speed and line-averaging of 9. Images were acquired at wavelengths corresponding to the λmax of the different dyes (405nm for DAPI, 488nm for FITC/Spectral green, 561nm for Spectral orange and 568 for Alexa fluor 568). Laser power and gain were adjusted so as to maximize the dynamic acquisition range for all the dyes. The image stacks were carefully examined using ZENlite 2011 and ImageJ softwares for image processing and quantification. Image pro plus (IPP v7.0) software was used for 3D reconstruction and radial distance analysis of chromosome territories. Percentage Radial distance of a chromosome territory (CT) is expressed as: (Distance of CT center from nuclear center)/ (Total distance from nuclear center to nuclear periphery)*100

8. siRNA transfection: siRNA used for Lamin A knockdown was: Lamin A2, 5'GCAAAGTGCGTGAGGAGTT3' (Sigma); siRNA used for Lamin B2 knockdown was Lamin B2.4, 5'-GCAAGUUUGUGCAGCUCAA-3'. 0.2 x 10^6 HEK293 cells were seeded to achieve a confluence of ~40% at 37°C, 5% CO_2. Cells were transfected with siRNA at 100 nM concentrations of oligos in OptiMem media (GIBCO) (250µl) and lipid (RNAimax from Invitrogen) - 5µl in 250µl OptiMem was left at RT for 30 min. Media was aspirated and cells were washed with Dulbecco's Phosphate Buffered Saline (DPBS) (GIBCO). 1.5ml DMEM media was added. After 30 min, 500µl of lipid+ siRNA mixture was added to the respective wells. Cells were incubated at

37°C incubator for 6 hr following which media was changed to DMEM. Cells were incubated at 37°C for 48 hr.

9. Primers: Primers used for RT PCR experiments are following:

Gene	Forward Primer	Reverse Primer
Lamin A	5'-CCGCAAGACCCTTGACTCA-3'	5'-TGGTATTGCGCGCTTTCA-3'
Lamin B2	5'-TGCGTGAGAATGAATGGG-3'	5'-ATAGTTTTCAGTGGCTCTGGG-3'
DNMT1	5'-CCCAGGATTACAAGGAAAAGC-3'	5'-CGATTTGGCTCTTTCAGACTC-3'
ACTIN	5'-GATTCCTATTGTGGGGGAC-3'	5'-GGTAGTCAGTCAGGTCCCG-3'
GAPDH	5'-CGAGATCCCTCCAAAATCAAG-3'	5'-GCAGAGATGATGACCCTTTTG-3'
GNL3L	5'-GATGCAGAAACGTGCAGATAAA-3'	5'-GGGAAGTGAGATCAGTCGATTAG-3'
CD99	5'-GGAGATGCTGTTGTTGATGGA-3'	5'-GGAGATGCTGTTGTTGATGGA-3'

10. RNA extraction:

(A) Lysate preparation with Trizol reagent: Media was removed from cells and were washed with 1XPBS. Cells were resuspended in trizol (500µl for 1.0X 10^6 cells) for 5 minutes at RT to allow complete dissociation of nucleoprotein complexes. Extensive washes were then performed by pipetting the suspension up and down.

(B) Phase separation: Chloroform (100 µl) was then added per 500 µl of the trizol reagent used. Contents of the tube were mixed by vigorous shaking for 15 seconds (no vortexing) and incubated at RT for 2-3 minutes. Sample was centrifuged at 12,000g for 15 minutes at 4°C. Colourless, upper phase (~300µl) containing the RNA was transferred to a fresh RNase free tube. Equal volume of ~ 70% ethanol added to obtain a final concentration of 35%.

(C) Binding, Washing & Elution: Ambion (life technologies, catalogue number: 12183018A) RNA purification kit used, following the manufacturer's protocol.

11. cDNA preparation:

Promega Kit of cDNA preparation utilized for cDNA synthesis (catalogue number: A3800).**(a)** Preparation of RNA mix:

Reagent	Stock Concentration (µg)	Final Concentration (µg)	Final Volume (µl)
RNA	Measured concentration	1	1-3
Oligo(dT) Primer	50	2.5	1
Nuclease free water (NFW)	-	-	2-4
Total Volume	-	-	5

(b) Preparation of Reverse transcription (RT) reaction mix:

Reagent	Stock concentration	Final Concentration	Final Volume (µl)
Nuclease-Free Water	-	-	final volume upto 15µl
IImprom-II Reaction buffer	5 X	1X	4.0
$MgCl_2$	25mM	3mM	2.4
dNTP Mix	10mM	0.5mM each	1.0
ImProm-II Reverse Transcriptase	20U	1U	1.0
RNasin	20U	0.5U	0.5
Total volume	-	-	15.0

Reactions tubes placed in a thermal cycler (eppendorf) and run the following PCR reaction:

I. 25°C – 15 minutes (Annealing)
II. 42°C- 60 minutes (Extension)
III. 70°C-5 minutes (Inactivation of Reverse transcriptase)
IV. 4°C- Hold

12. Quantitative Real time PCR:

(a) Preparation of Master mix: Master mix was prepared for a total volume of 9 µl containing each of the components below:

Reagent	Stock Concentration	Final Concentration	Final Volume (µl)
Kapa Syber Green (KAPA Biosystems, Catalogue number: KM4100)	5X	1X	5.0
Primer	10µM	0.25 µM	0.4
Nuclease free water	_	_	3.6
Total volume	-	-	9.0

Master mix was vortexed gently, and kept on ice prior to dispensing into the reaction tubes. cDNA dilutions were then prepared and 1 µl added to master mix to make net volume 10 µl of each tube.

(c) Preparation of controls (in duplicates):

Controls	Nuclease free water (µl)	Primer (µl)	cDNA (µl)	Kapa Syber green (µl)	Total volume (µl)
Water control	5.0	-	-	5	10
cDNA control	4 .0	-	1	5	10
Primer control	4.6	0.4	-	5	10

(d) Experimental setup and run: 10 µl of each primer and control mastermixes with cDNA added in the respective well in a 96well PCR plate. The plate sealed with microsealer with the help of soft tissue by gently pressing the tube.

Run the qRT-PCR instrument under following conditions:

I. 95°C**-** 5 minutes-Hot start reaction
II. 95°C- 20 seconds**-** Denaturation
III. 60°c- 1 minute- Annealing and Data acquisition (40 cycles)
IV. Insert melt curve: Determination of melt curve
V. 4^{o}C- Hold
VI. The run takes~ 1hour 45 minutes

(e) Running the samples on agarose gel: PCR products were resolved in a 1.5% agarose gel at 100V for 2 hours

Loading setup:

Sample	5µl
6X loading dye	1µl

Syber safe DNA gel stain (Invitrogen, catalogue number: S33120) was added 5µl per 100ml of the agarose gel. Gel was observed and imaged under G:Box System from 'SYNGENE' using 'Genesnap' software.

13. Whole cell lysate preparation and protein estimation: 0.6-0.8 x 10^6 cells were seeded in each well of 6 well plate and incubated overnight at 37°C incubator. Following morning, media was aspirated and cells were washed with 1X DPBS. Cells were trypsinized with 500 µl of 0.05 % trypsin-EDTA mix (GIBCO) and left in CO_2 incubator for 5 min. After that, cells were flushed in 500µl of DMEM and centrifuged at 1000 rpm for 5 min. Supernatant was discarded and pellet was re-suspended in appropriate amount of media. Cells were counted using a Hemocytometer by mixing 1µl of trypan blue in 9µl of cells suspension. The cells were then washed in ice cold 1X PBS. Cells were centrifuged at 1000 rpm for 5min. Supernatant was discarded and 75µl of RIPA+PIC was added. Cells were incubated on ice for 15 min under gentle rocking. Cells were then centrifuged at 14000g for 15 min. Supernatant was transferred to fresh microfuge tube and flash frozen in liquid N_2 and stored at -80°C. For protein estimation, cell lysates were thawed on ice and estimated using Pierce BCA protein estimation kit. BSA Standards of concentration ranging from 2mg/ml to 0.25mg/ml (10µl/well) were used. Lysates were diluted to 1:2 with 1X PBS. RIPA buffer were diluted to 1:2 with 1X PBS served as blank. Reagents A and B (50:1) were mixed and 200 µl of it was added to each well. The plate was wrapped with aluminum foil and incubated at 37°C for 30 min. Optical density was then measured using spectrophotometer at 562nm. Absorbance curve was plotted using BSA standards, which was then used to calculate the concentration of proteins in the lysate.

14. SDS-PAGE and western blotting:

The whole cell lysate was resolved in a 12% polyacrylamide gel.

Sample preparation: Loading mixture was prepared in 1X PBS and 1X Laemmli buffer. Sample was denatured by incubating at 95°C for 10 min. 8 µl of All Blue (ladder) and 4 µl of magic marker added. The gel was resolved at a constant voltage of 120V. Transfer was performed under cold conditions. PVDF membrane was cut appropriately and activated in methanol and washed with distilled water twice. Transfer was set up for 90 min at 90 V. Two TBST washes of 10 min each were

given and then left in 5% non-fat dried milk for blocking for 1 hr. Abcam Mouse anti Lamin A (dilution 1:2000) or Abcam Mouse anti Lamin B2 (1:2000) or Rabbit anti GAPDH (1:5000), primary antibody in 0.5% skimmed milk were added to blot and incubated for 3 hr at RT. The blot was washed 3 times in 1X TBST and then incubated in 1:5000 sheep anti mouse or 1:10000 goat anti rabbit IgG HRP (prepared in 0.5% skimmed milk) for 1 hr at RT. Three TBST washes were then given for 5 min each. Blot was then developed using chemiluminescence.

15. BAC DNA extraction

BAC clones for the candidate genes (*XIST*, *FOXP3*) were retrieved from UCSC genome browser and purchased from BACPAC resources (*XIST*: RP11-13M9, *FOXP3*: RP11-1037C20). The clones were grown in chloramphenicol (12.5µg/ml). The colonies were inoculated in 5ml LB-chloramphenicol culture and allowed to grow for 6 hours and this pre-innoculum was expanded into 500 ml LB-chloramphenicol medium. The culture was grown for 16 hours following which the BAC DNA was extracted using Hi Pure plasmid filter Maxi prep kit from Invitrogen (Life technologies, Reference number: K210017) eluted in 200 µl TE buffer (pH=8.0). The DNA was quantified using the Nanodrop at 260 nm.

16. Probe preparation: The required dUTP labeled DNA probes, for the genes *XIST* and *FOXP3* were prepared by nick translation using the kit from Roche Applied Sciences (Product number:10976776001), following the manufacturer's protocol.

17. Composition of different reagents/ buffers:

(a) 10XPBS (amount in for 1000ml):

Component	**Amount (in gm)**
Na_2HPO_4	12.90
$NaH_2PO_4.H_2O$	2.30
NaCl	90

Bring to final volume using dd H_2O when 1X PBS is made. pH is 7.2 before autoclaving after autoclaving it increases.

(b) 10X TBS (for 1000ml):

Component	Amount
Tris	60.5gm
NaCl	87.6gm
Distilled water	(to make volume up to 1 litre)

(c) 10X Running buffer (for 1000ml):

Component	Amount (in gm)
Tris	30.30
Glycine	144
SDS	10

Make up volume using distilled water

(d) 1X Transfer buffer (for 1000ml):

Component	Amount
Tris	5.82gm
Glycine	2.92gm
20% SDS	1.86ml
Methanol	200ml
Distilled water	800ml

(e) 1X washing buffer (for 1000ml):

Component	Volume (in ml)
5 M NaCl	27
Tris HCl (pH 7.4)	8
Tween 20	1

Make volume up to 1000ml

(f) Blocking solution for blot: 5% Non fat milk powder in TBST. 0.5% is further dilution in TBST

(g) 20X SSC (for 1000ml):

Component	Amount (in gm)
NaCl	175.3
Na- citrate.$2H_2O$	88.2

Adjust pH to 7.06 using HCl and adjust volume to 1000ml with distilled water

(h) 50% Formamide-2XSSC (for 100ml):

Component	Volume (in ml)
98% Formamide	51
20X SSC	10

Adjust final volume up to 1000ml with distilled water. Adjust pH to 7.4

(i) RIPA buffer (for 200 ml):

Component	Volume
1M Tris-Cl	100ml
1M NaCl	20ml
10% Na-azide	0.2ml
Na- deoxycholate	1gm
Np-40	2ml
0.5 M EDTA	0.4ml
SDS (0.1%)	0.2gm

(j) 12% resolving gel composition:

Component	Amount
Distilled water	2.5ml
30% acryl amide	3ml
Tris (pH 8.8)	1.9ml
20% SDS	37.5µl
10% APS	75µl
TEMED	3µl

(k) 4% stacking gel composition:

Component	**Volume**
Distilled water	1.4ml
30% acryl amide	330µl
Tris (pH 6.8)	250µl
20% SDS	10µl
10% APS	20µl
TEMED	2µl

(l) 4X Laemmli buffer (for 12 ml):

Component	**Volume (in ml)**
0.5 M Tris (pH 6.8)	4.4
Glycerol	4.4
20% SDS	2.2
1% Bromophenol Blue	0.5
β –Marcaptoethanol (ME)	0.5

18. Statistical analysis: The data obtained from experiments and analysis on Image Pro Plus software were subjected to statistical analysis on Graphpad Prism (version 6.0) and Microsoft excel (v 2007). Unpaired analysis of fluorescent intensity and qRT PCR data was performed using two tailed student t-test. Unpaired analysis of percentage radial distance data was performed using Kolmogorov-Smirnov (KS) test which could capture subtle differences in radial distribution. Unpaired analysis of chromosome territory and nuclear topological features like volume and surface area was performed using Mann-Whitney (MW) test. Z test of proportion was applied on genomic loci fish data to examine statistical significant difference. A value of $p<0.05$ is considered statistically significant.

CHAPTER 3

Results

The aim of this project is to examine the effect of Lamin A and Lamin B2 depletion on nuclear structure and function relationship in HEK293 cells. More specifically we attempted to examine the role of lamins in maintaining position of inactive X chromosome territory and all X chromosome territories. We also examined the relative spatial location of CT 18 (gene poor, peripheral) and CT 19 (gene rich, central) in HEK293 cells. Further; nuclear volume, CT volume and surface area, gene expression levels and gene loci positioning (*FOXP3* gene of X chromosome) were tested in Lamin A and Lamin B2 depleted cells. The overall goal was to examine the role of Lamin A and Lamin B2 knockdown in exerting its effect on X chromosome and also on CT 18 and 19 in an aneuploid cell line.

1. Identification of a cell line as a model for studying X-chromosome positioning: Multiple cell lines were initially screened for their karyotype and presence of inactive X chromosomes in order to identifying a cell line with at least one X chromosome and stable karyotype. SW480 human colorectal cancer cells, MCF7 human breast cancer cells and HEK293 human embryonic kidney cells were examined for this purpose. These cell lines were subjected to inverse DAPI metaphase banding to examine karyotype and immunostaining for inactive X chromosome (Xi) marker proteins to identify inactive X chromosome. Metaphase FISH assay was utilized to assess number of X chromosome present in some of these cell line.

(A) SW480 cells

Ploidy analysis of SW480 cells: SW480 cell line has been derived from male colorectal cancer tissue (Leibovitz et al., 1977). In order to establish karyotype of these cells metaphases were generated from these cells followed by DAPI staining as described in (material and methods section 4). These DAPI stained metaphases were observed and imaged under a fluorescence microscope. Images were analyzed to assess the karyotype based on inverse DAPI banding. Karyotyping reveals a modal chromosome number of 48 (n=10) (Figure 3.1 (a) & (b)).

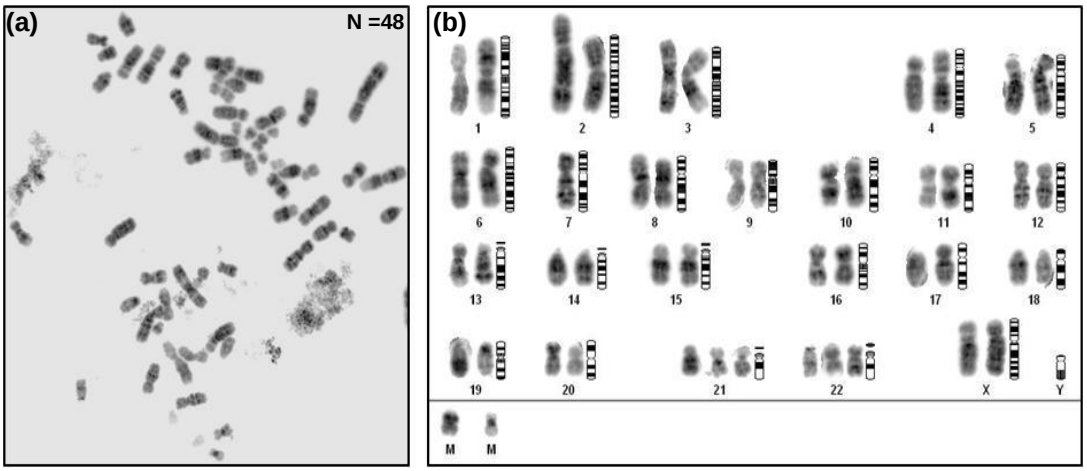

Figure 3.1: Ploidy determination of SW480 cells. **(a)** Representative inverse DAPI stained metaphase of SW480 cells. **(b)** Representative karyotype of SW480 metaphase (inverse DAPI banding).

Absence of Xi markers in SW480 cells: SW480 cells exhibit loss of Y chromosome and presence of two X chromosomes. However, very little is known about the transcriptional activity of these X chromosomes (Melcher et al., 2000). These X chromosomes can either follow dosage compensation mechanism which implies having one active and one inactive X chromosome; or they can have two copies of active X chromosome by a candidate mechanism of 'isodisomy' (Engel et al., 1980). Isodisomy is a mechanism which leads to two copies of a uniparental chromosome in usually cancer cells. We sought to examine the presence of inactive X chromosomes in SW480 cells by performing an immunostaining for Xi markers H3K27me3 and macroH2A. Confocal images do not exhibit any specific staining of these markers (Figure 3.2). These results indicate that inactive X chromosome is absent in SW480 cells.

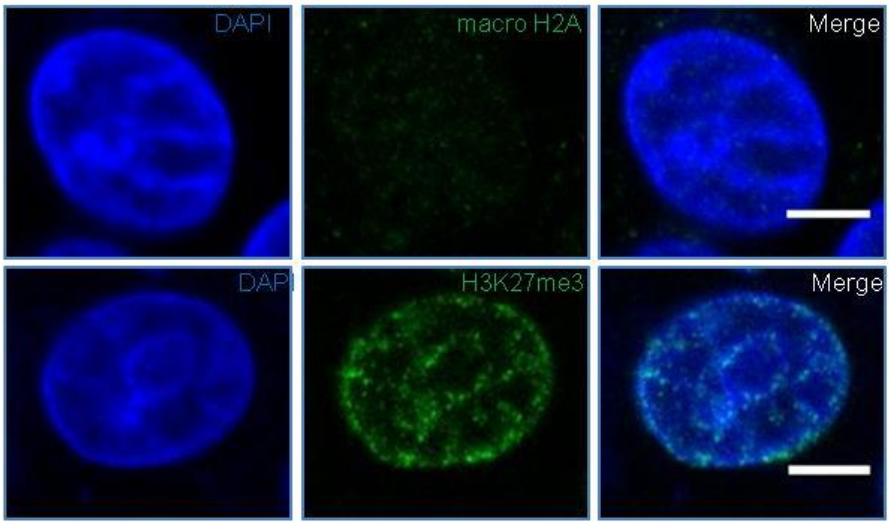

Figure 3.2: Sub-nuclear positioning of Xi markers in SW480 cells. Immunostaining of H3K27me3 and macro H2A in SW480 cells. Scale bar: 5μm.

Localization of CT X and Nucleolus: SW480 cells were utilized in order to develop an assay to visualize DNA and protein simultaneously. This assay was performed for whole chromosome paint for CT X and Nucleolin - a nucleolar protein. Cells were first immunostained with anti-Nucleolin antibody, followed by hybridization with WCPX the following day. Confocal images show localization of CTX and Nucleolin in the same nuclei by ImmunoFISH (Figure 3.3). This assay would enable us to discriminate active from inactive X chromosome if whole chromosome fluorescent paint and macro H2A antibody are used. Since macro H2A labels Xi in interphase nuclei; chromatin regions where both CTX and macro H2A colocalize would represent Xi and only CTX signal would correspond to active X chromosome territory.

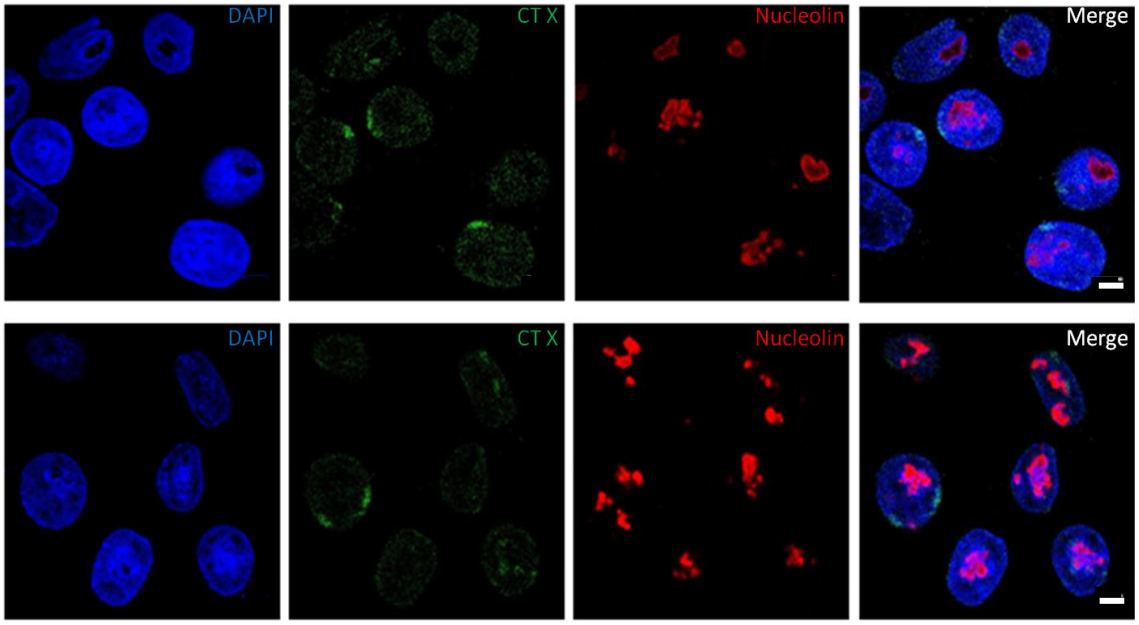

Figure 3.3: Intranuclear localization of X chromosome territory (CT X) and nucleolar marker protein Nucleolin SW480 cells. Scale bar: 5µm.

(B) MCF7 cells:

Ploidy analysis of MCF7 cells: MCF7 cells were derived from breast epithelial cancer tissue. These cancer cells have a heterogeneous population of multiple active and inactive X chromosomes (Winnard et al., 2006). In order to establish ploidy of MCF7 clone, inverse DAPI karyotyping was performed. Metaphase preparation and DAPI staining was performed according to protocol mentioned in materials and methods section 4. These DAPI stained metaphases were observed and imaged under fluorescence microscope. Images were analyzed to assess the karyotype based on inverse DAPI banding using 'Applied Imaging Software (ASI)' software (Figure 3.4 (a) & (b)). Karyotyping reveals a modal chromosome number of 71 (n=60). MCF7 cells show a hypertriplod karyotype (Figure 3.4 (c)).

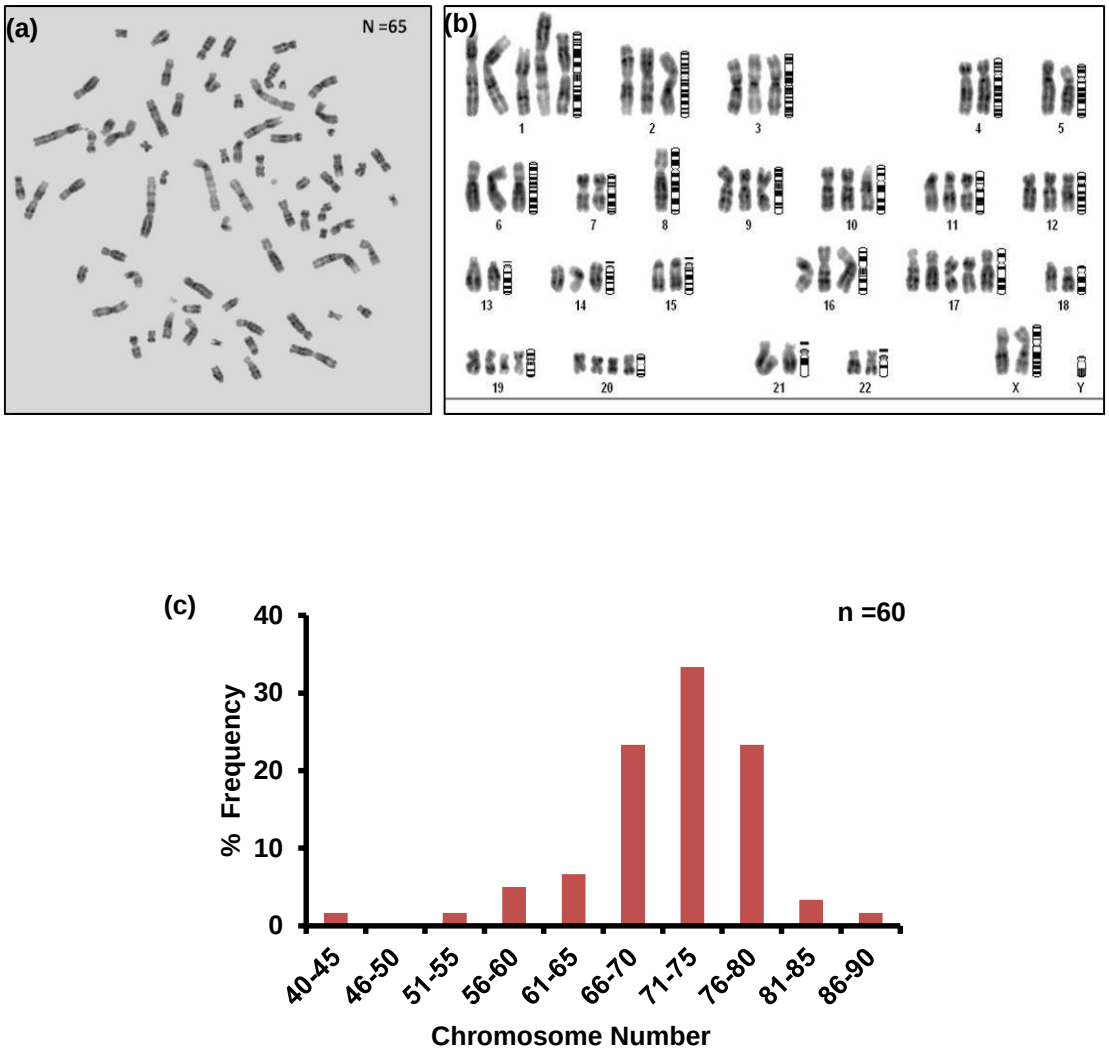

Figure 3.4: Ploidy analysis of MCF7 cells. **(a)** Representative inverse DAPI stained metaphase of MCF7 cells. **(b)** Representative karyotype of MCF7 metaphase (inverse DAPI banding). **(c)** Percentage frequency distribution of chromosome number of MCF7 cells based on inverse DAPI banding.

MCF7 cells exhibit Xi markers: We next sought to examine the presence of Xi in MCF7 cells by immunostaining for H3K27me3 and macro H2A. These cells were immunostained for Lamin A, macro H2A and H3K27me3. Images were acquired on confocal microscope and processed on Image J software. These images reveal presence of Lamin A at the nuclear periphery and large foci of H3K27me3 and macro H2A in the interior of the nucleus (Figure 3.5). The specific staining of macro H2A and H3K27me3 confirm the presence of Xi.

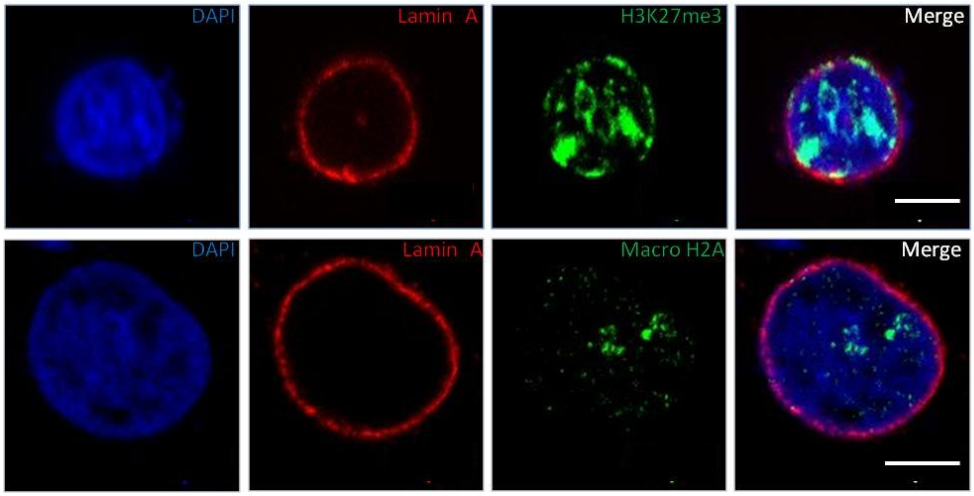

Figure 3.5: Sub-nuclear positioning of Xi markers in Lamin A knockdown MCF7 cells. Immunostaining of Lamin A, H3K27me3, and Macro H2A in untreated and Lamin A KD MCF7 cells. Scale bar: 5.0 µm.

(C) HEK293 cells:

Ploidy analysis of HEK293 cells: HEK293 cells were derived from human (female) embryonic kidney (Graham et al., 1977). In order to establish ploidy of HEK293 cell line, inverse DAPI karyotyping was performed. Metaphase preparation and DAPI staining was performed according to protocol mentioned in materials and methods section 4. These DAPI stained metaphases were observed and imaged under fluorescence microscope and analyzed using ASI software (Figure 3.6 (a) & (b)). Karyotyping reveals a modal number of 60 chromosomes (n=50). HEK293 cells demonstrate a hypotriploid karyotype (Figure 3.6 (c)).

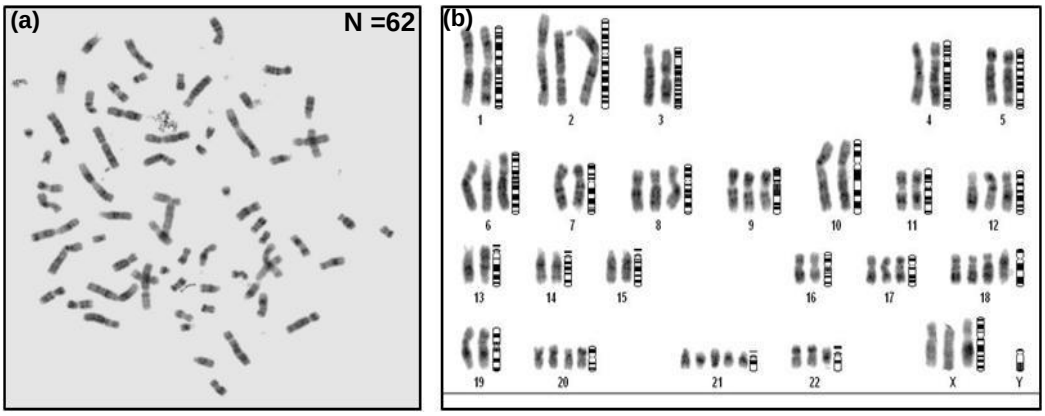

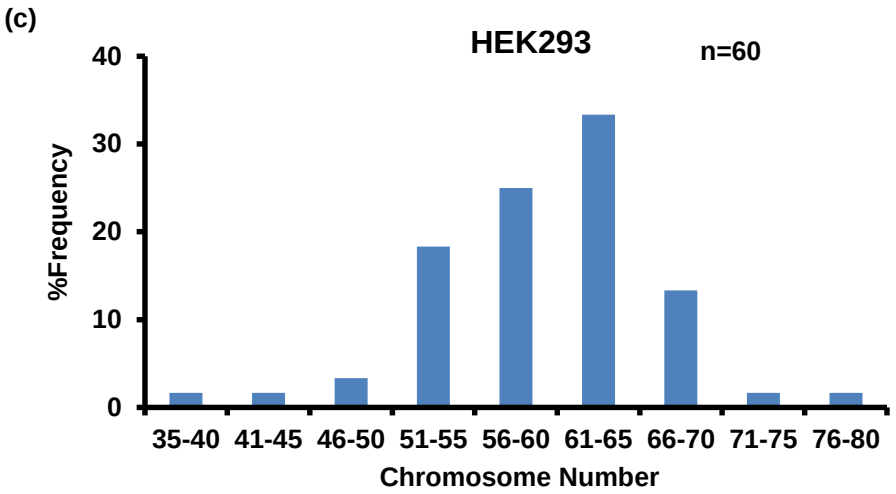

Figure 3.6: Ploidy analysis of HEK293 cells. **(a)** Representative inverse DAPI stained metaphase of HEK293 cells. **(b)** Representative karyotype of HEK293 metaphase (inverse DAPI banding). **(c)** Percentage frequency distribution of chromosome number of HEK293 cells based on inverse DAPI banding.

Determination of X chromosome numbers in HEK293 cells: We sought to examine the modal number of X chromosomes in HEK293 cells by metaphase FISH. Metaphase spreads were generated and were subjected to FISH. Whole chromosome paints for chromosome X and chromosome 18 were used for hybridization and metaphases were counterstained with DAPI. These metaphases were observed and imaged under fluorescence microscope (Figure 3.7(a)). Numbers of X chromosomes were enumerated per metaphase and a frequency was plotted (n= 50), (Figure 3.7(b)). HEK293 cells predominantly show four X chromosomes (~80%) and a smaller subpopulation of three X chromosomes (~ 20%)

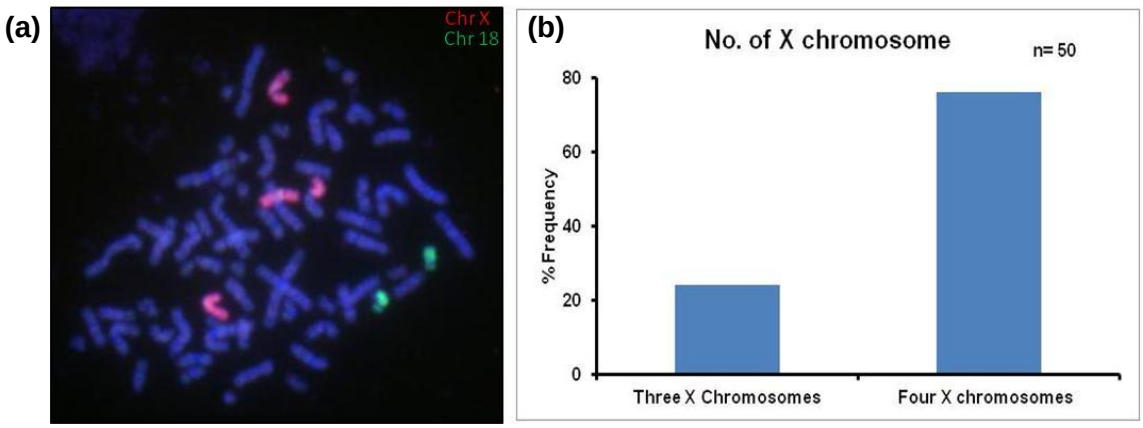

Figure 3.7: Determination of number of X chromosomes in HEK293 cells. **(a)** Metaphase FISH on HEK293 cell for chromosome X and chromosome 18. **(b)** Total no. of X chromosomes in HEK293 metaphases from metaphase FISH.

HEK293 cells were used for rest of the experiments:

2. Intranuclear localization of Xi in lamin knock down cells:

2.1 Effect of Lamin A and Lamin B2 depletion on Xi positioning: To examine the effect of Lamin A depletion in intranuclear positioning of inactive X chromosome immunofluorescence assay was performed for untreated and Lamin A KD cells. HEK293 cells were subjected to Lamin A knockdown and stained with Lamin A, macro H2A and H3K27me3. Confocal imaging shows a uniform and peripheral staining of Lamin A at the nuclear membrane in untreated cells and presence of specific foci for H3K27me3 and macro H2A (Figure 3.8 (a)). There is ~80% reduction in fluorescent intensity of Lamin A in Lamin A knockdown cells ($p<0.005$, paired student t test, Figure 3.8 (b)) which confirms knockdown of Lamin A in these cells. Similar experiments were performed for Lamin B2 KD (Figure 3.8 (c)). Fluorescent intensity was quantified and it displays ~70% reduction in of Lamin B2 intensity in Lamin B2 KD cells ($p<0.005$ unpaired two tailed student t-test) (Figure 3.8 (d)).

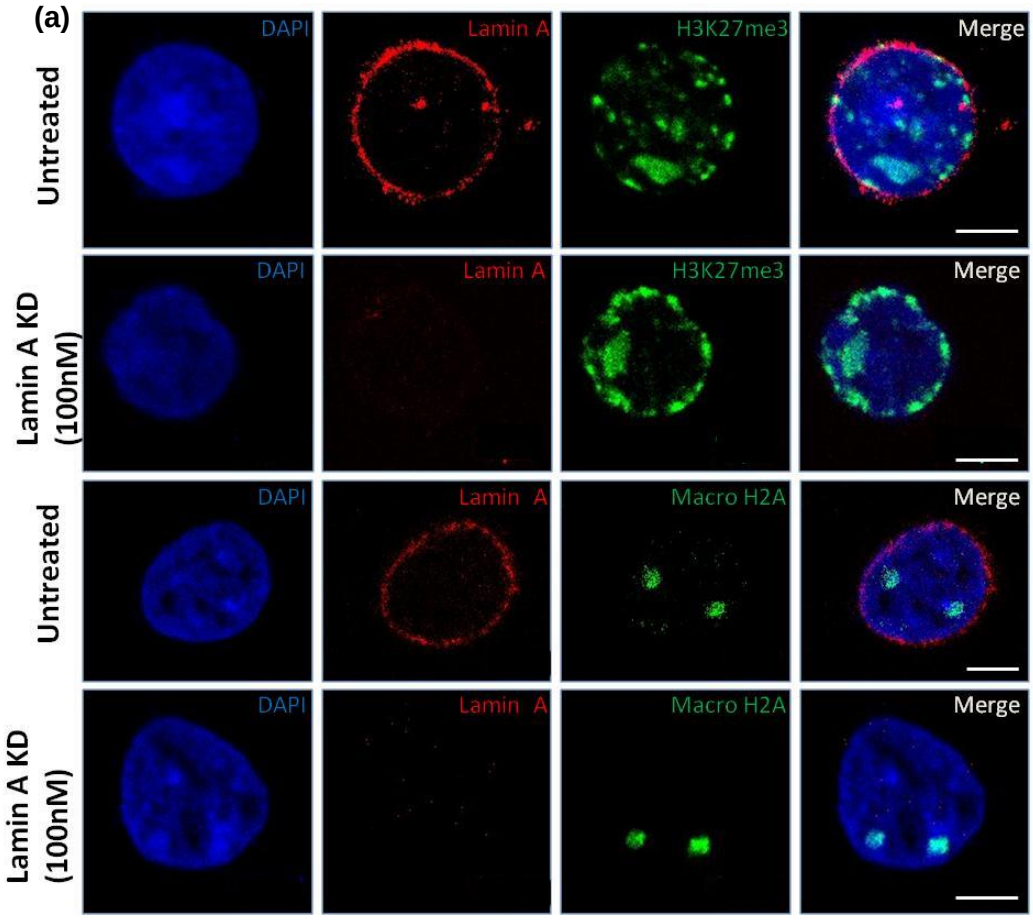

(b)

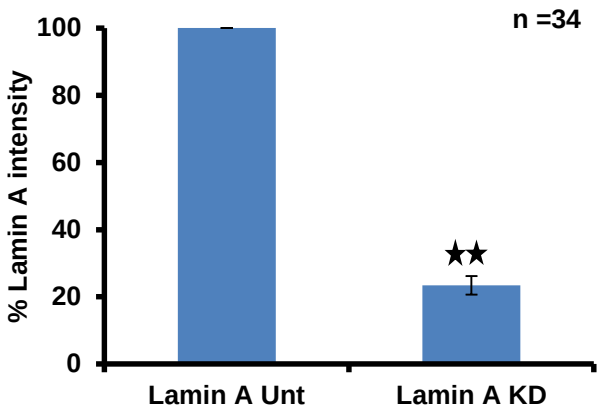
n =34
100
80
60
40
20
0
% Lamin A intensity
★★
Lamin A Unt
Lamin A KD

(c)

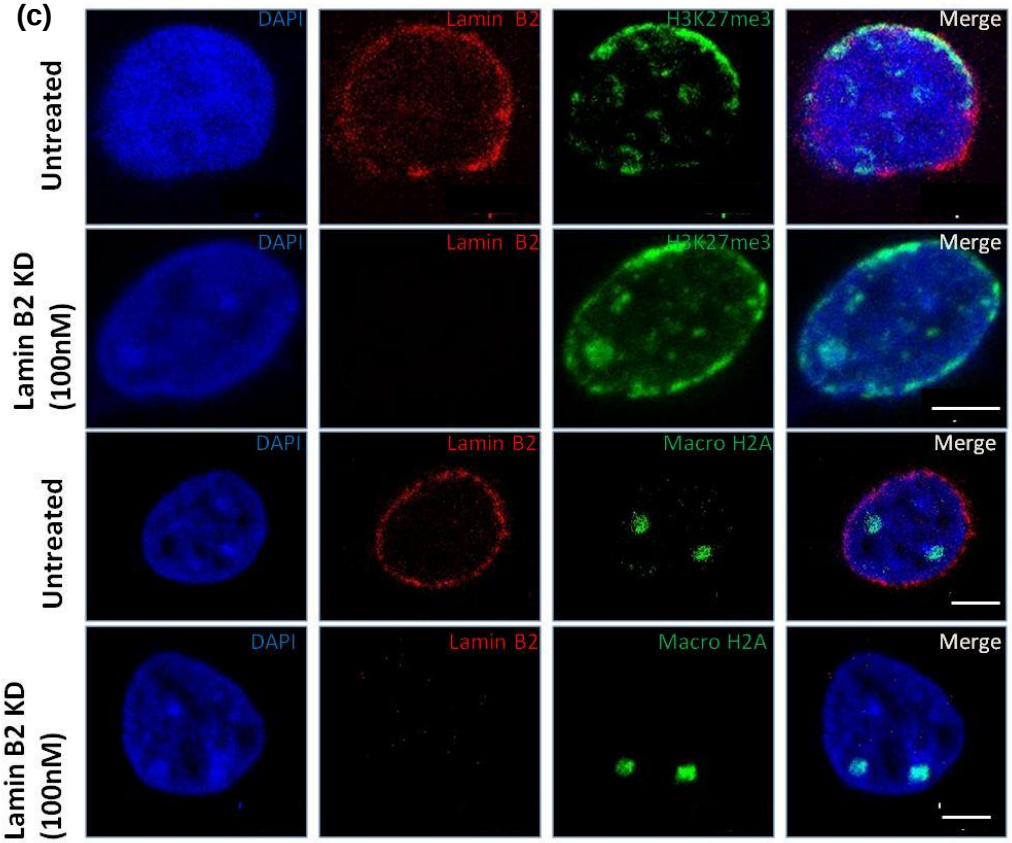
Untreated
Lamin B2 KD (100nM)
Untreated
Lamin B2 KD (100nM)
DAPI
Lamin B2
H3K27me3
Macro H2A
Merge

(d)

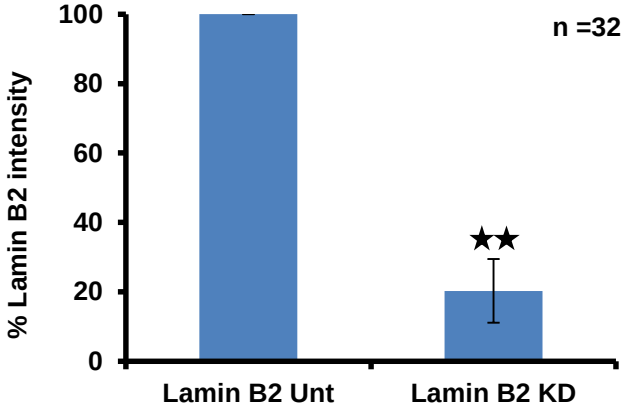
n =32
100
80
60
40
20
0
% Lamin B2 intensity
★★
Lamin B2 Unt
Lamin B2 KD

Figure 3.8: Xi markers in Lamin A and Lamin B2 depleted cells. **(a)** Sub-nuclear positioning of Xi markers in Lamin A knockdown HEK293 cells. Immunostaining of Lamin A, H3K27me3, and Macro H2A in untreated and Lamin A KD HEK293 cells. Scale bar: 5.0 µm. **(b)** Levels of Lamin A fluorescence intensity in HEK293 nuclei after Lamin A knockdown. **(c)** Subnuclear positioning of Xi markers in Lamin A knockdown HEK293 cells. Immunostaining of Lamin B2, H3K27me3, and Macro H2A in untreated and Lamin A KD HEK293 cells. Scale bar: 5µm. **(d)** Levels of Lamin B2 fluorescence intensity in HEK293 nuclei after Lamin B2 knockdown. ★★: $p < 0.005$ (paired student t test).

Knockdown of Lamin A and Lamin B2 was confirmed with western blot analysis. Whole cell protein extract were prepared from untreated, Lamin A scrambled, Lamin A KD, Lamin B2 scrambled and Lamin B2 KD HEK293 cell (Materials and methods section 13). 25 µg of whole cell extract was resolved in 10% SDS-PAGE gel and subjected to western transfer and probed with mouse anti-Lamin A and mouse anti Lamin B2 antibodies independently (materials and methods section 14). The same blot was reprobed with Rabbit anti GAPDH antibody as a loading control. Significant decline in Lamin A and Lamin B2 levels was observed upon knockdown (Figure 3.9 (a) & (b)) which confirms depletion of lamins in these cells.

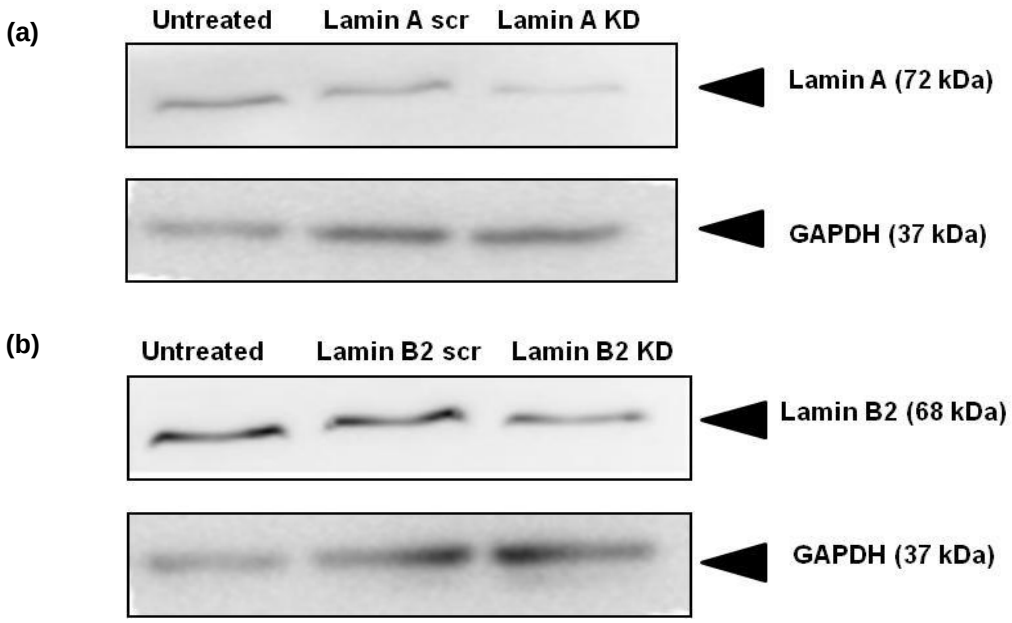

Figure 3.9: Western blot for **(a)** Lamin A KD and Lamin B2 KD **(b)** siRNA mediated knockdown of Lamin A, B2 at 100 nM siRNA oligo concentration. GAPDH used as loading control.

Imaged nuclei were then subjected to 3D reconstruction and radial positioning analysis using Image Pro Plus (IPP v7.0) software. Macro H2A is exclusively present in inactive X chromosome and hence it would be utilized for Xi radial positioning analysis. Percentage radial distances, nuclear volume, Xi volume, nuclear surface area and Xi surface area were estimated from 3D reconstructed images of untreated, Lamin A KD and LaminB2 KD HEK293 cells. This does not exhibit any significant change in radial distances for Lamin A KD ($p>0.05$, Kolmogorov- Smirnov (KS) test) but a significant decrease in radial distances was detected for LaminB2 KD ($p<0.05$,

Kolmogorov-Smirnov (KS) test) (Figure 3.10(a) and Table 1). There is no significant change in Xi volume in Lamin A KD cells ($p>0.05$, MW test) while there is significant decrease in Xi volume in LaminB2 KD cells ($p<0.05$, MW test) (Figure 3.10 (b) and Table 1). Xi surface area distribution shows changes in both Lamin A and LaminB2 depleted cells. Lamin A KD cells show a decrease in surface area of Xi ($p<0.0005$, MW test) whereas Lamin B2 KD reveals a significant increase in surface area of Xi ($p<0.0005$, MW test) (Figure 3.10 (c) and Table 1).

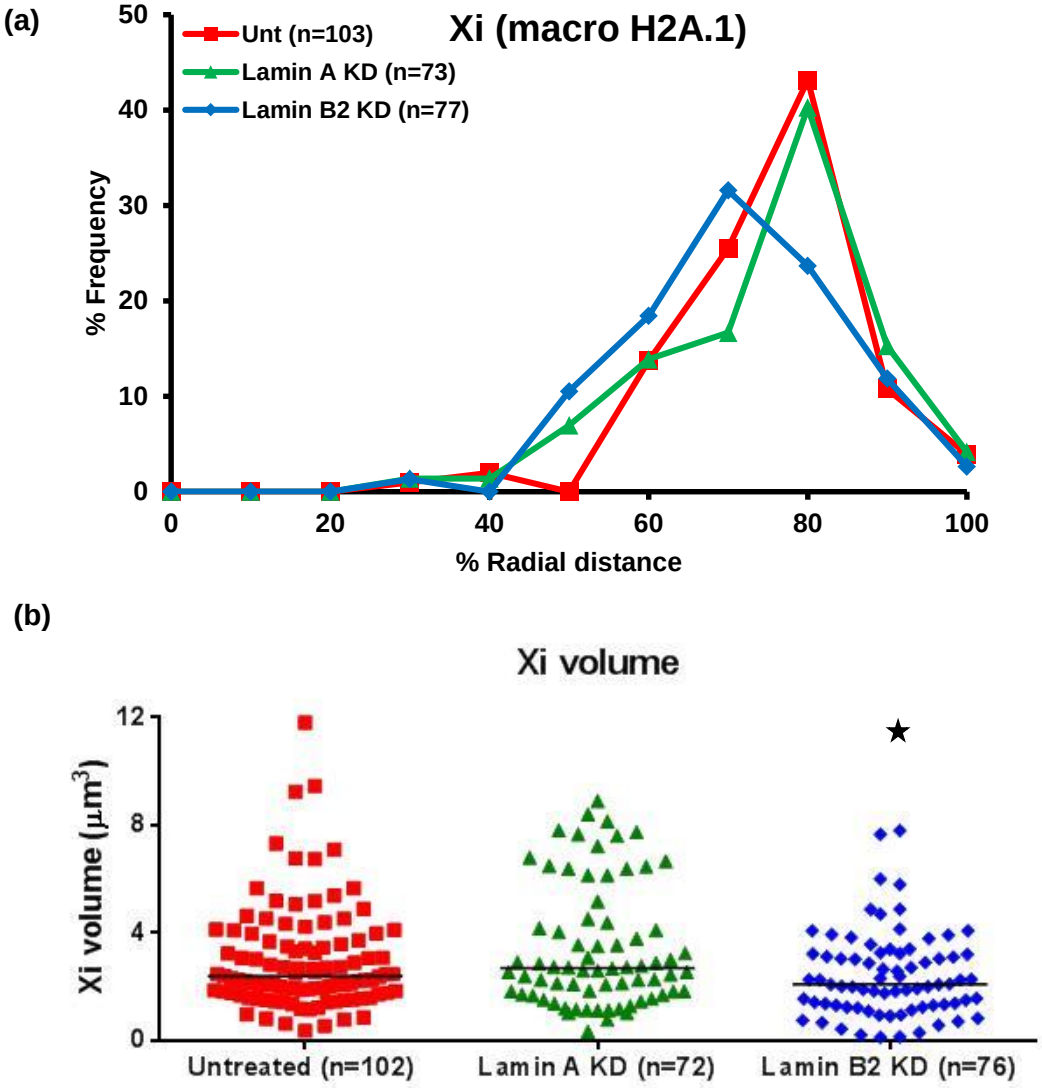

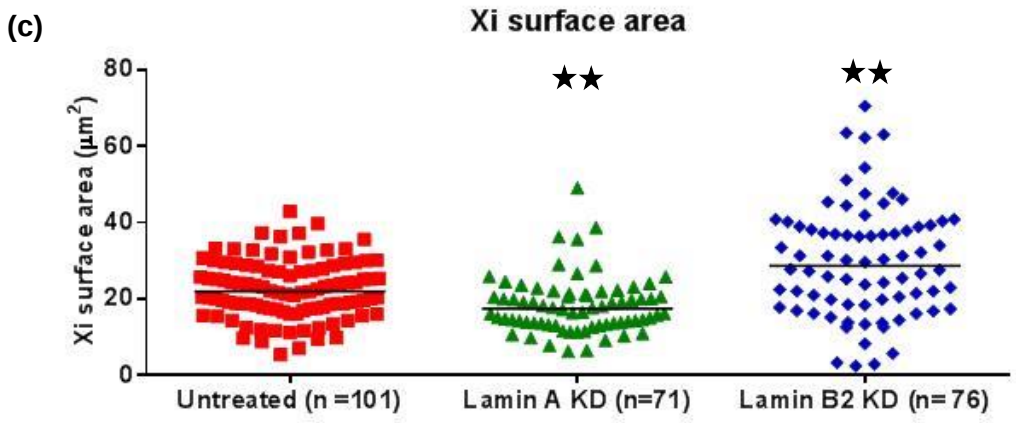

Figure 3.10: Effect of LaminA and LaminB2 depletion on inactive X chromosome. **(a)** Percentage radial distance distribution of percentage radial distance of untreated, Lamin A KD and Lamin B2 KD Xi territory based upon macro H2A staining. **(b)** Distribution of Xi volume in untreated, Lamin A and Lamin B2 knock down HEK293 cells. **(c)** Distribution of Xi surface area in untreated and Lamin A knock down HEK293 cells. Middle line in all scatter plots represent median. n is number of chromosome territories. ★: $p<0.05$; ★★: $p<0.005$.

3. Intranuclear localization of CTX, CT18 and CT19 in Lamin depleted cells- Radial distance, volume and surface area measurements of CTs:

After examining sub-nuclear localization of Xi we sought to examine the effect of Lamin knockdown on positioning of candidate chromosome territories. Chromosome X, 18 and 19 were selected for this purpose. Chromosome 18 (gene poor chromosome) is located towards the periphery of the nucleus. Chromosome 19 is a gene rich chromosome, and hence is more centrally located (Croft et al., 1999). X-chromosome is in either active or inactive transcription state, where inactive X always localizes towards nuclear periphery (Heard et al., 2005).These properties of chromosomes make them ideal candidates to study effect of Lamin depletion on chromosome territories.

Lamin A and Lamin B2 knockdown was performed on HEK293 cells and after 48 hours was processed for 3D-FISH and hybridized with fluorescently labeled whole chromosome paints for chromosome X, chromosome 18 and chromosome 19 territories. Confocal images were acquired and Image processing and analysis was performed using Image Pro Plus and Image J applications. These images reveal presence of specific territories of these chromosomes (Figure 3.11 (a) & 3.11 (b)).

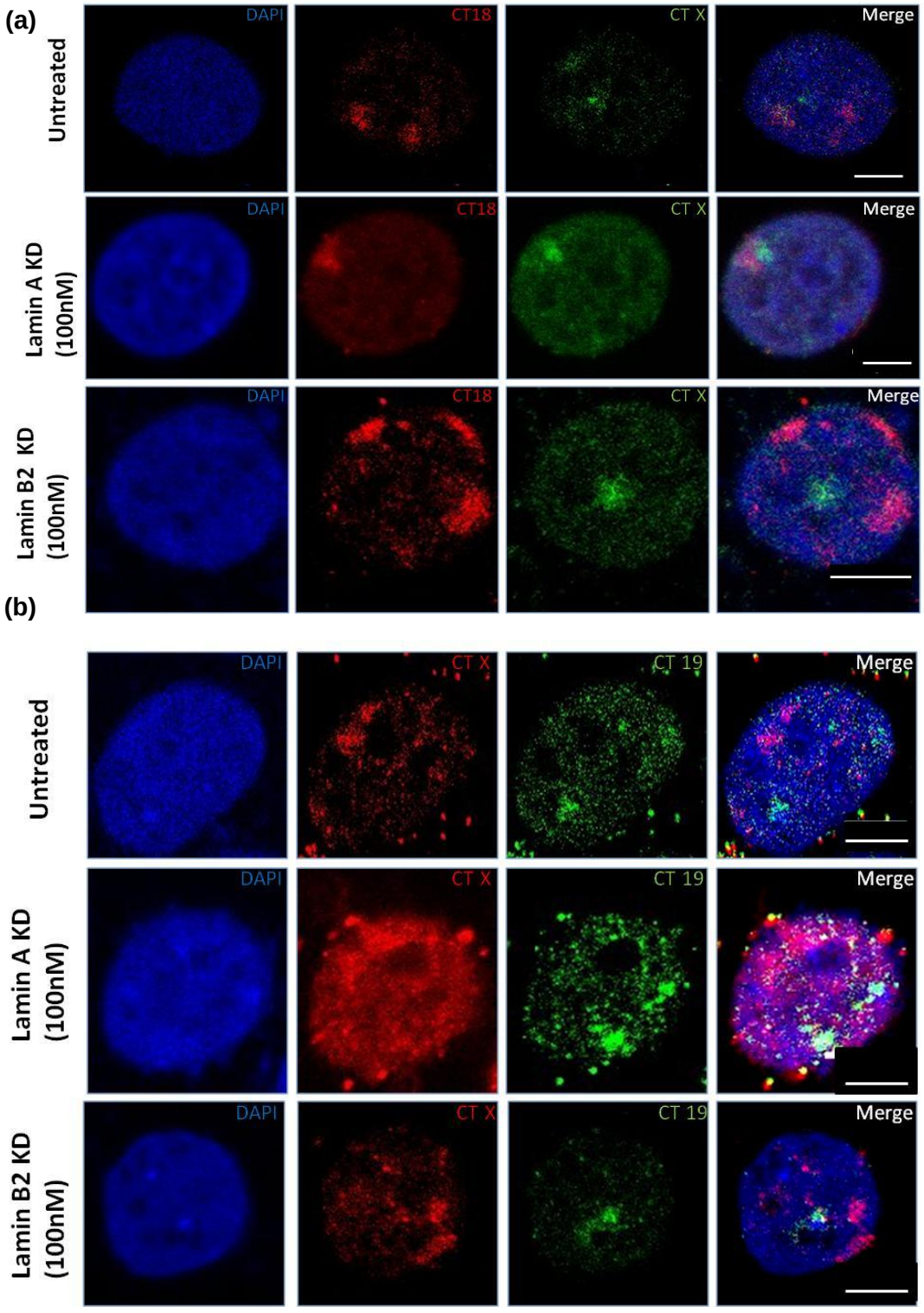

Figure 3.11: (a) intranuclear positioning of CT X and CT18 in Lamin A and Lamin B2 Knock down HEK293 cells based on fluorescent in situ hybridization (3D- FISH) of chromosome specific probes for CT X and CT 18. **(b)** Intranuclear positioning of CT X and CT19 in Lamin A and Lamin B2 Knock down HEK293 cells based on fluorescent in situ hybridization (3D-FISH) of chromosome specific probes for CT X and CT 19. Scale bar: 5µm.

3D reconstruction and analysis of specific territories was performed on Image Pro Plus software to estimate radial distances, territory volume and territory surface area. Chromosome X territory does not (inclusive of active and inactive X CTs) displays significant change in its radial positioning upon Lamin A and Lamin B2 depletion ($p>0.05$, Kolmogorov-Smirnov (KS) test) (Figure 3.12 (a) and Table 1). CT X volume and surface area also does not show any significant difference in Lamin A and Lamin B2 depleted cells ($p>0.05$, Mann Whitney (MW) test, Figure 3.12 (b) and table 1).

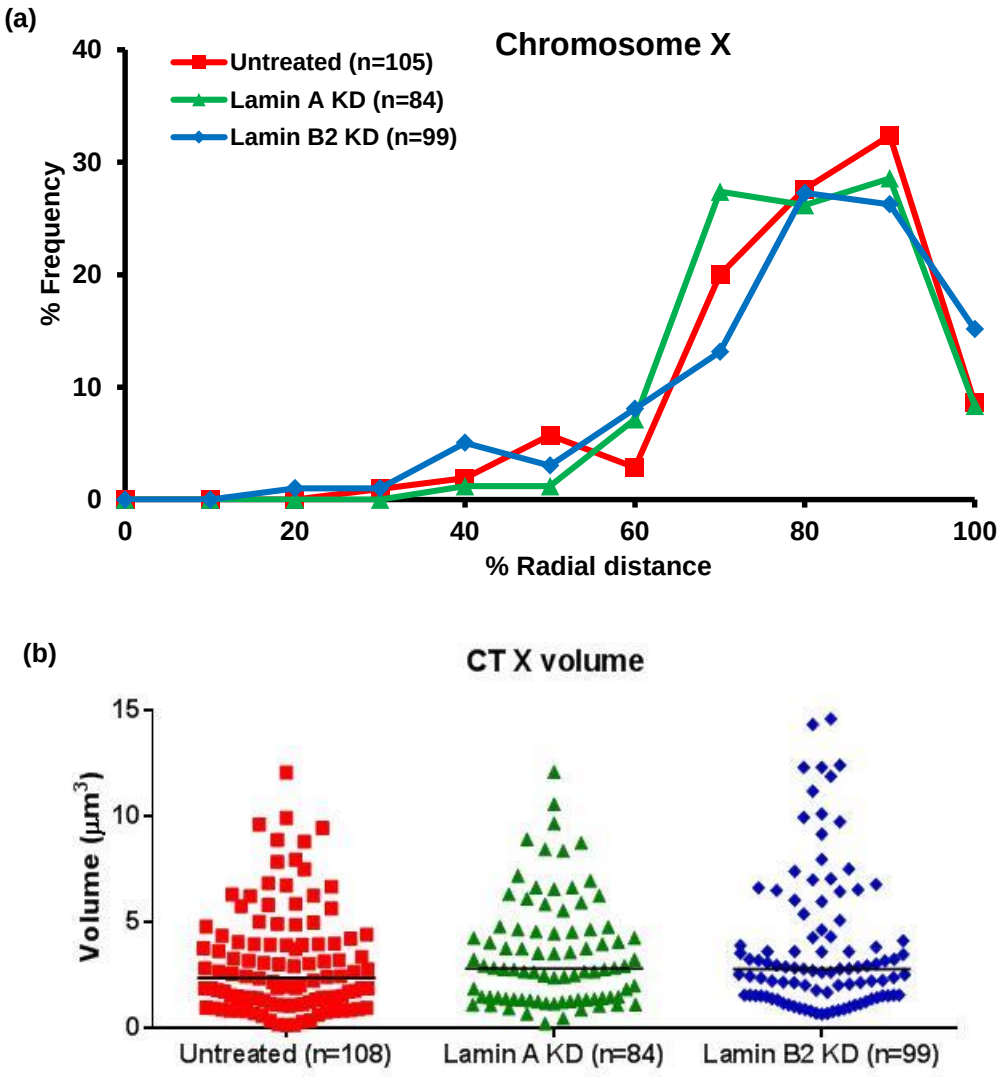

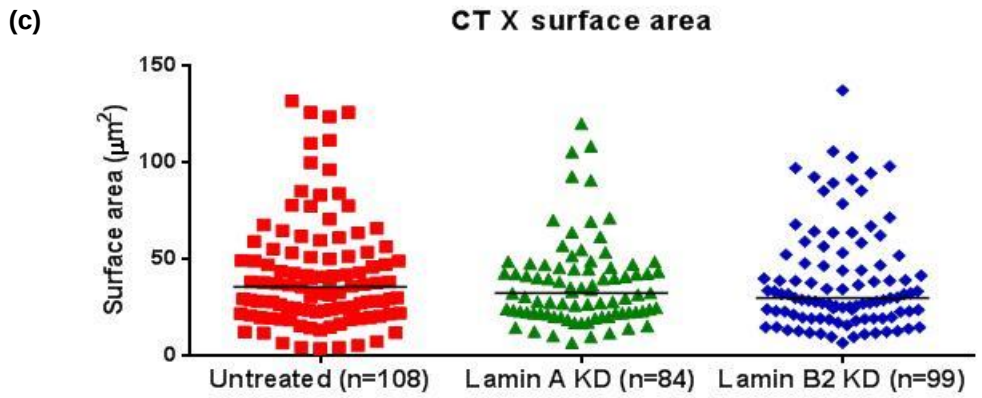

Figure 3.12: Effect of Lamin A and Lamin B2 depletion on different parameters associated with CT X. **(a)** Percentage radial distance distribution of percentage radial distance of untreated, Lamin A KD and Lamin B2 KD chromosome X territory. **(b)** Distribution of CT X volume in untreated, Lamin A and Lamin B2 knock down HEK293 cells. **(c)** Distribution of CT X surface area in untreated, Lamin A KD and Lamin B2 knock down HEK293 cells. Middle line in all scatter plots represent median. n is number of chromosome territories.

Radial distance distribution of CT18 reveals no significant change in Lamin A depletion ($p>0.05$, KS test) but a significant alteration in Lamin B2 depleted cells ($p<0.05$, KS test, Figure 3.13(a) and Table 1). Chromosome territory volumes remain unaltered in both lamin depleted cells ($p>0.05$, MW test, Figure 3.13(b) and Table 1). CT18 surface area in Lamin B2 KD cells exhibit significant decline compare to untreated ($p<0.005$, MW test), while Lamin A depletion shows no significant change in surface area ($p>0.05$, MW test) (Figure 3.13(c) and Table1).

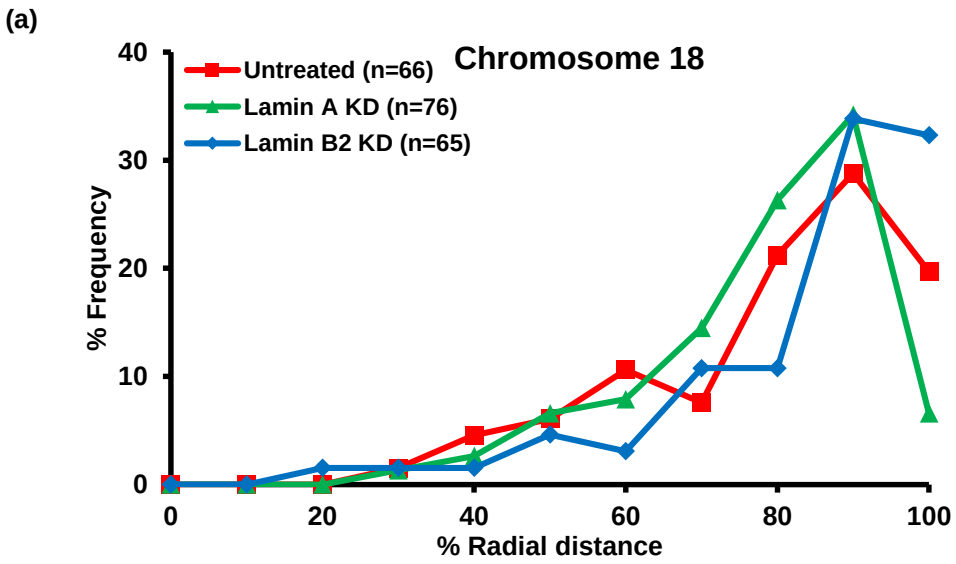

(b)

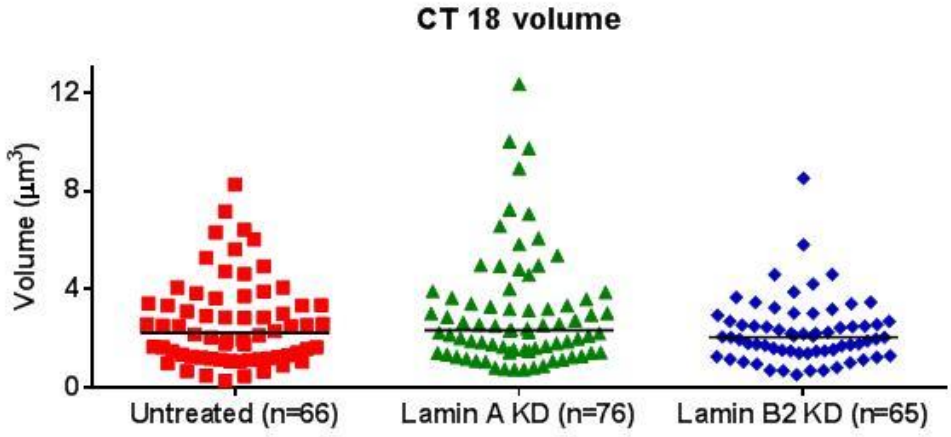

(c)

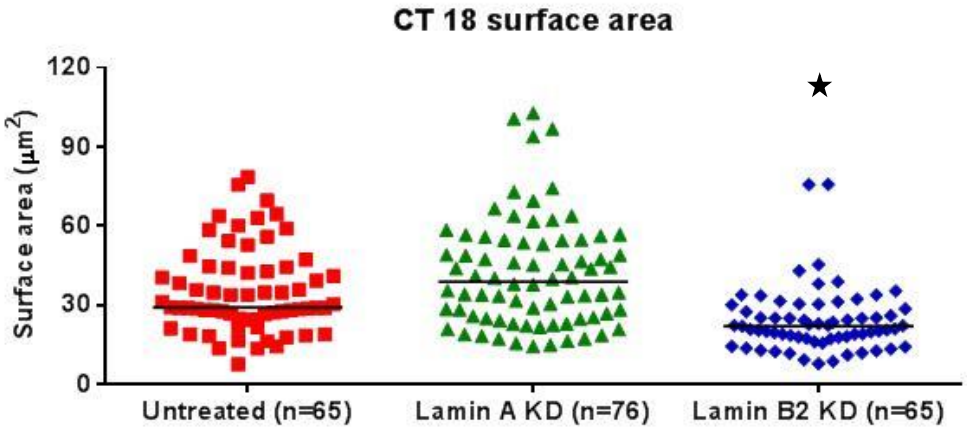

Figure 3.13: Effect of Lamin A and Lamin B2 depletion on different parameters associated with CT 18. **(a)** Percentage radial distance distribution of percentage radial distance of untreated, Lamin A KD and Lamin B2 KD chromosome 18 territory. **(b)** Distribution of CT 18 volume in untreated, Lamin A and Lamin B2 knock down HEK293 cells. **(c)** Distribution of CT 18 surface area in untreated, Lamin A KD and Lamin B2 knock down HEK293 cells. Middle line in all scatter plots represent median. n is number of chromosome territories. ★: $p<0.05$.

CT19 does not exhibit significant alteration in percentage radial distance for both Lamin A and Lamin B2 depleted cells ($p>0.05$ for both, KS test) (Figure 3.14(a) and Table 1). CT19 volume remains unaltered in Lamin A KD cells ($p>0.05$, MW test) whereas there is significant decline in CT19 volume in Lamin B2 depleted cells ($p<0.05$, MW test) (Figure 3.14(b) and Table 1). CT19 surface area is not significantly affected in Lamin A KD cells ($p>0.05$, MW test); while Lamin B2 KD shows very significant decline in surface area ($p<0.005$, MW test) (Figure 3.14(c) and Table 1).

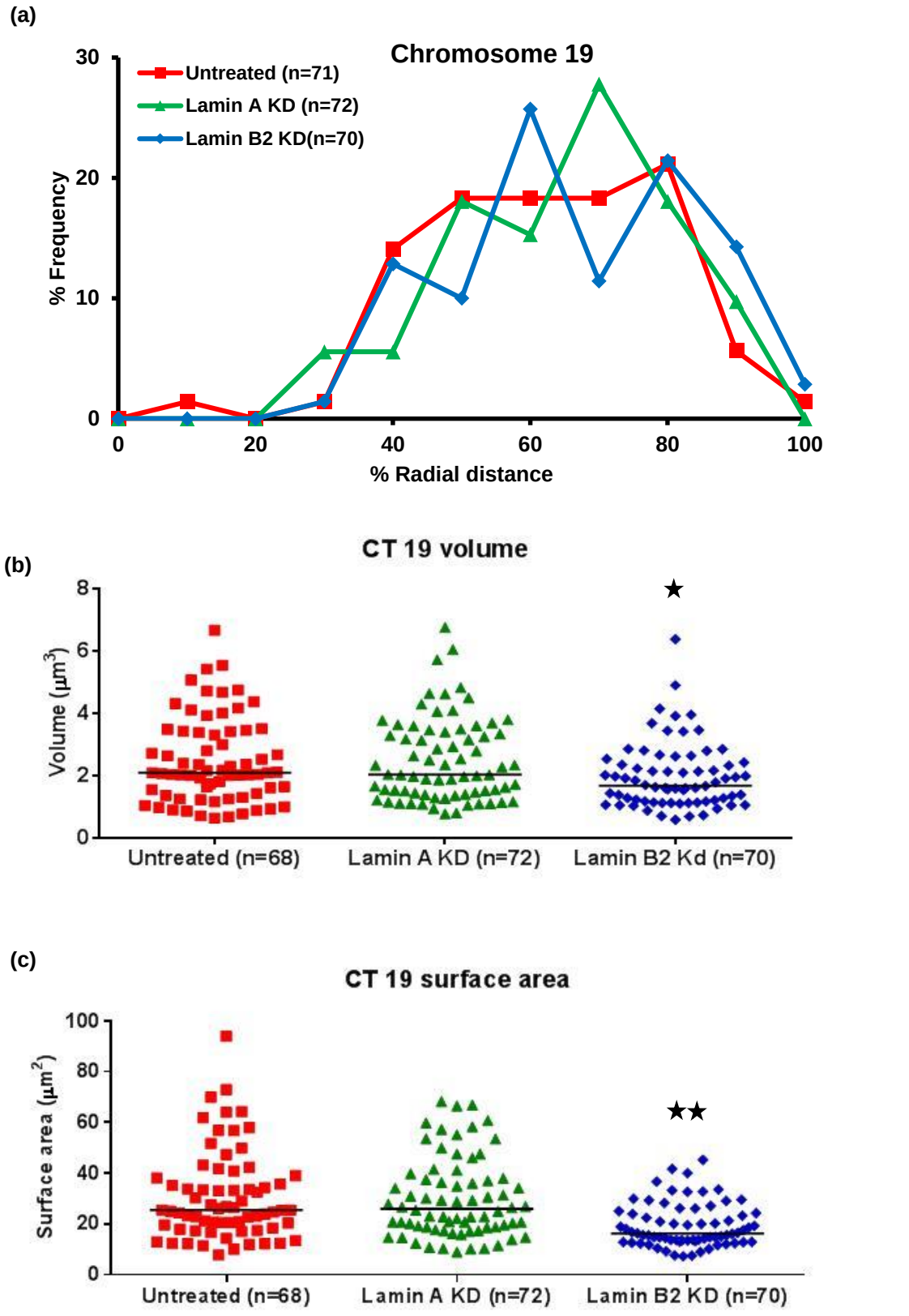

Figure 3.14: Effect of Lamin A and Lamin B2 depletion on different parameters associated with CT 19. **(a)** Percentage radial distance distribution of percentage radial distance of untreated, Lamin A KD and Lamin B2 KD chromosome 19 territory. **(b)** Distribution of CT 19 volume in untreated, Lamin A and Lamin B2 knock down HEK293 cells. **(c)** Distribution of CT 19 surface area in untreated, Lamin A KD and Lamin B2 knock down HEK293 cells. Middle line in all scatter plots represent median. n is number of chromosome territories. ★:p<0.05; ★★:p< 0.005.

4. Effect of lamin depletion on nuclear volume and nuclear surface area:

In order to examine if Lamins affect overall nuclear topology; nuclear volume and surface area measurements were performed on 3D reconstructed nuclei from confocal images using Image Pro Plus software. Lamin A KD nuclei reveal significant decrease in nuclear volume ($p<0.05$, MW test) whereas Lamin B2 KD does not show a significant change ($p>0.05$, MW test) (Figure 3.15 (a) and Table 1). However, neither Lamin A nor Lamin B2 depletion leads to any significant change in nuclear surface area ($p>0.05$, MW test) (Figure 3.15 (b) and Table 1).

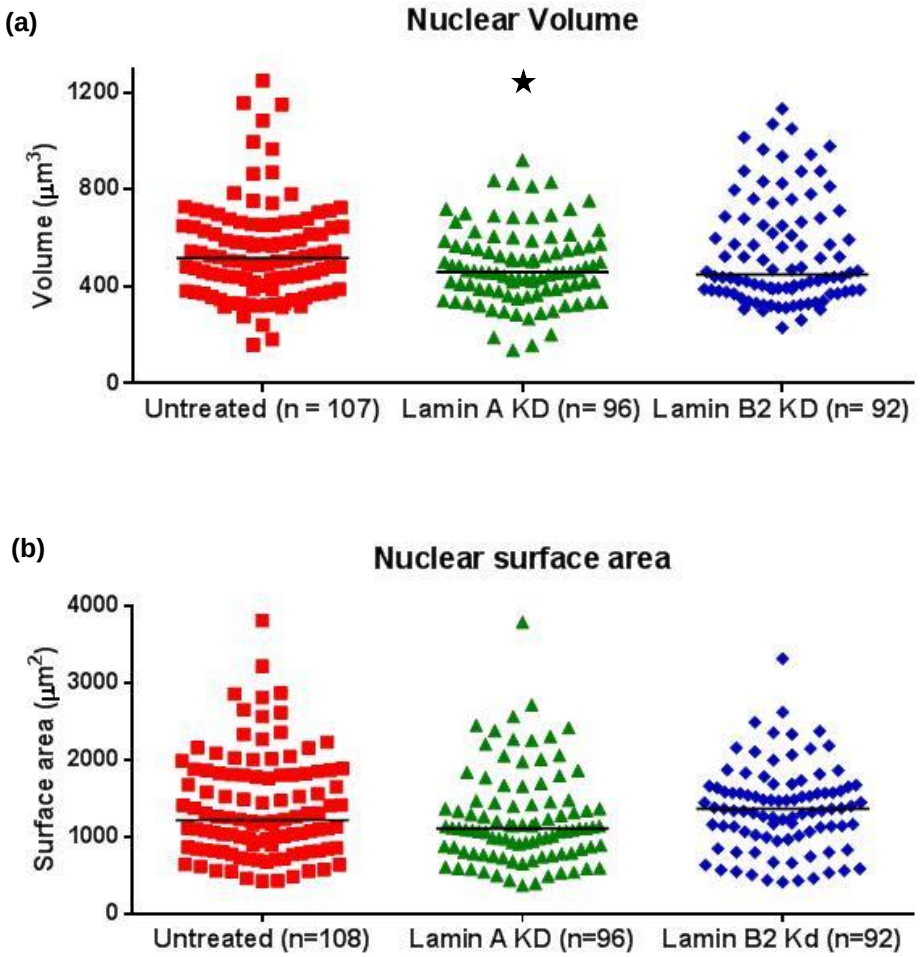

Figure 3.15: Effect of lamin depletion on nuclear architecture. **(a)** Nuclear volume in untreated, Lamin A KD and Lamin B2 KD HEK293 cells. **(b)** Nuclear surface are in untreated, Lamin A KD and Lamin B2 KD cells. Middle line in all scatter plots represent median. n is number of nuclei. ★: $p<0.05$.

Data obtained from percentage radial distance measurement, volume and surface area measurements are shown in Table 1.

Chromosome territory	Sample	Radial Distance (percentage)	Volume (μm^3)	Surface area (μm^2)
CT Xi	Untreated	M=71.91	M=2.380	M=21.92
	Lamin A KD	M=73.48, p=0.6835	M=2.689, p=0.3242	**M=17.40, p<0.0001**
	Lamin B2 KD	**M=64.86, p=0.0024**	**M=2.086, p=0.0494**	**M=28.71, p=0.0004**
CT X	Untreated	M=77.64	M=2.371	M=32.42
	Lamin A KD	M=74.74, p=0.9612	M=2.809, p=0.1519	M=35.61, p=0.4253
	Lamin B2 KD	M=77.12, p=0.9142	M=2.787,p=0.0919	M=29.86, p=0.3794
CT 18	Untreated	M=77.92	M=2.349	M=29.09
	Lamin A KD	M=75.82, p=0.4642	M=2.234, p=0.3919	M=39.90, p=0.0811
	Lamin B2 KD	**M=84.44, p=0.0185**	M=2.057, p=0.4065	**M=21.97, p<0.0001**
CT 19	Untreated	M=59.11	M=2.103	M=25.51
	Lamin A KD	M=61.53, p=0.8285	M=2.040, p=0.9705	M=25.99, p=0.8197
	Lamin B2 KD	M=59.74, p=0.7052	M=1.687, p=0.8197	**M=16.27, p<0.0001**

Table 1: Summary of data obtained for percentage radial distance measurement, volume and surface area for chromosome territories. M: median of the distribution; p: p value from KS or MW test. Text in bold represents significant difference ($p<0.05$) compared to untreated.

5. Effect of lamin depletion on nuclear localization of *FOXP3* gene loci with respect to CT X:

We next examined spatial localization of *FOXP3* loci (Chr.Xp11.23) in three dimensionally preserved HEK293 cells. The aim of this experiment was to specifically examine if lamin depletion affects 3D localization of genes with respect to their chromosome territory. Lamin A and Lamin B2 knockdown was performed on HEK293 cells and after 48 hours processed for 3D-FISH and hybridized with fluorescently labelled whole chromosome paints and fluorescently labelled probes of gene loci. Confocal images were acquired and the location of *FOXP3* gene loci was enumerated by examining its location vis-à-vis chromosome X territory. Three distinct loci states were identified (i) Inside (ii) Peripheral and (iii) Outside with respect to X chromosome territory (Figure 3.16 (a)). Numbers of loci present in each state were enumerated in untreated, Lamin A KD and Lamin B2 KD cells (Figure 3.16 (b)). Z-test of proportions was applied to all values and only in Lamin B2 KD *FOXP3* gene loci was significantly 'Outside' relative to untreated cells.

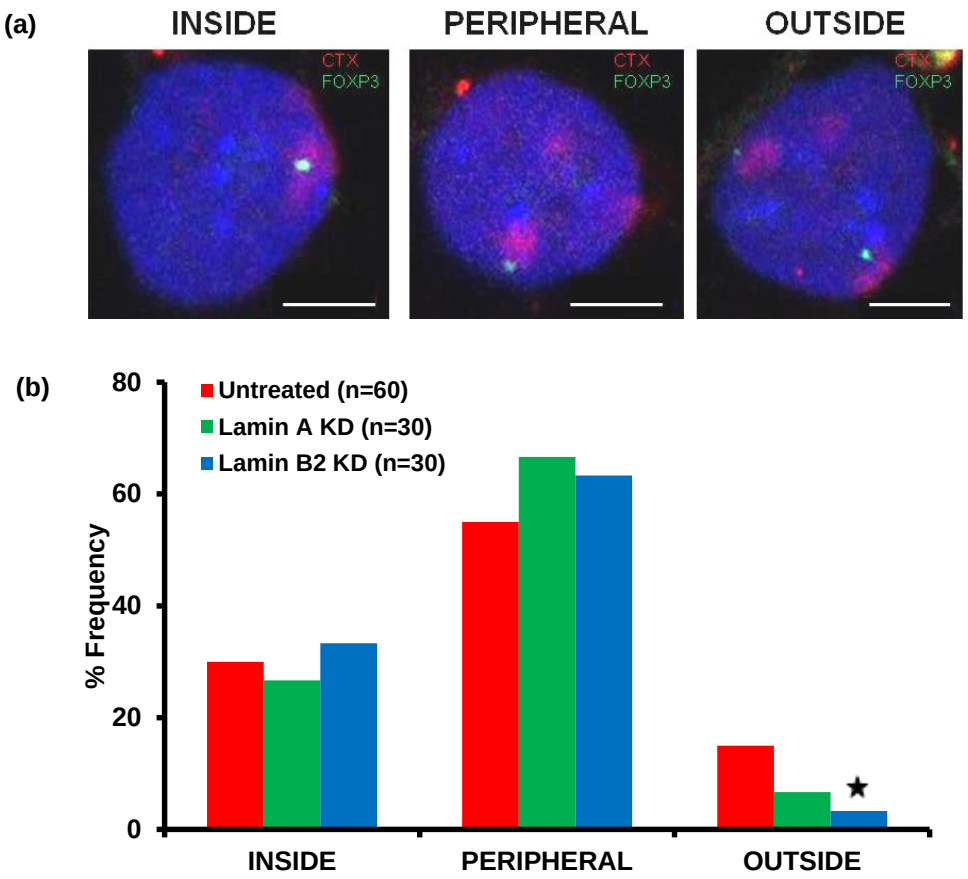

Figure 3.16: Effect of lamin depletion on gene loci positioning. **(a)** Confocal image projections of 3D FISH performed on HEK293 cells. *FOXP3* displays three distinct loci states with respect to CT X. Scale bar: 5µm. **(b)** Quantification of loci positioning in untreated and lamin depleted cells. ★: $p<0.05$.

5. Transcript levels of X linked and DNA methylation maintenance gene in lamin depleted HEK293 cells:

We next sought to examine transcript levels of genes present on X chromosome. These genes can be divided into two categories: (i) genes silenced during X inactivation process (ii) genes with Y chromosome homologue that do not show transcriptional silencing on inactive X chromosome. These second category of genes are located on pseudoautosomal region (PARs). Candidate gene selected from transcriptionally silent region in inactive X chromosome is *GNL3L* and gene selected from pseudoautosomal region is *CD99*. Specific primers for these genes were designed and tested for their efficiency. These primers were then utilized to assess gene expression levels of candidate genes. *DNMT1* is DNA methyltransferase responsible for maintenance of DNA methylation on inactive X chromosome. In order to assess transcriptional status of these genes in Lamin A and Lamin B2 depleted HEK293 cells real time PCR experiment was carried out for three technical replicates (Figures 3.17).

Lamin A knock down data demonstrate significant decrease in Lamin A levels ($p< 0.005$, unpaired two tailed student t-test) which confirms the efficiency of siRNA

mediated knockdown of Lamin A. *DNMT1* and *GNL3L* levels also show significant decrease in gene expression levels ($p<0.005$ and $p<0.05$ respectively, unpaired two tailed student t-test). However there is no significant change in pseudoautosomal region gene *CD99* ($p>0.05$). Actin was used as internal control to normalize C_t value.

Lamin B2 knockdown and RT-PCR was performed similarly. *GAPDH* was used as an internal control to normalize C_t values. Lamin B2 knock down data demonstrate a significant decline in Lamin B2 levels ($p<0.005$, paired two tailed student t-test) which confirms the efficiency of siRNA mediated knockdown of Lamin B2. *DNMT1* and *GNL3L* levels also shows a significant decrease in gene expression levels ($p<0.005$ in both, unpaired two tailed t-test).

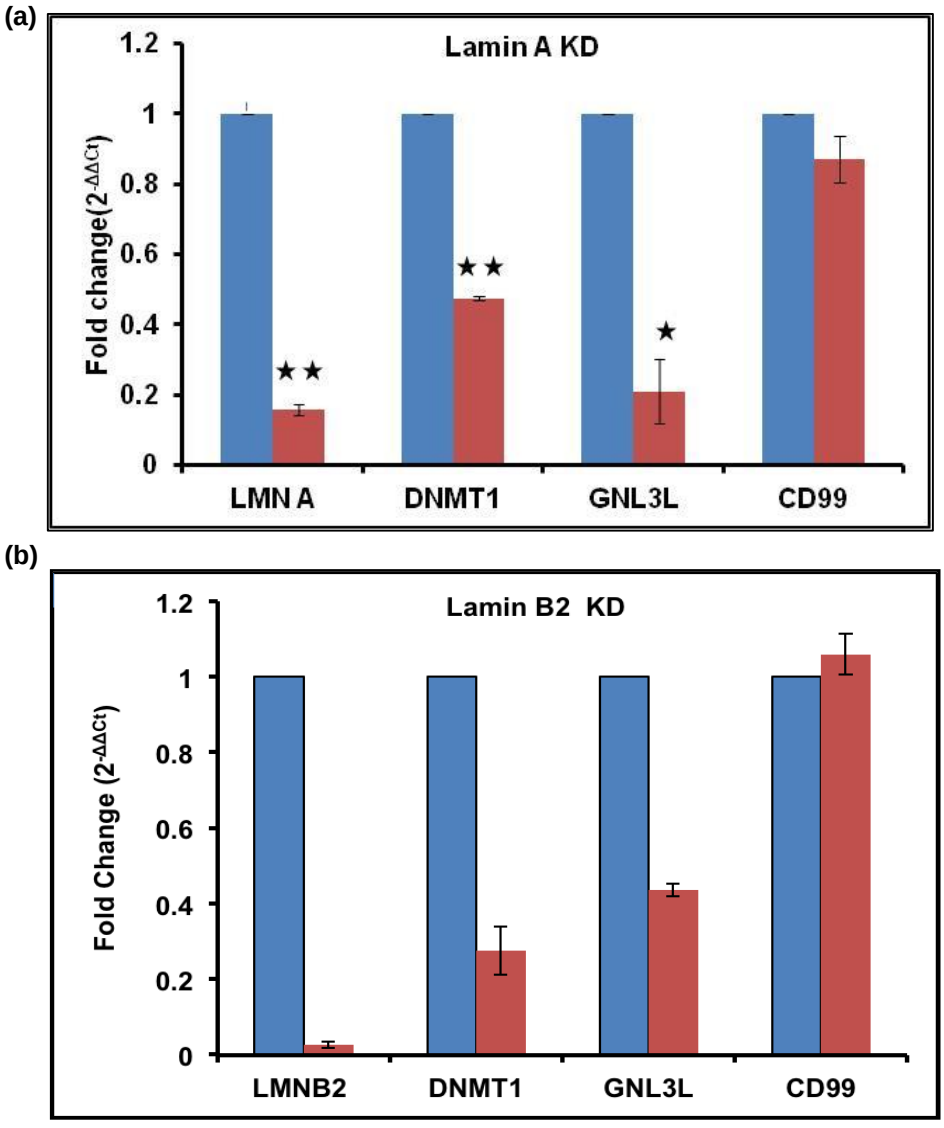

Figure 3.17: Transcript levels of Lamin A, Lamin B2, DNMT1, GNL3L and CD99 genes in (a) Lamin A knockdown HEK293 cells (b) Lamin B2 knockdown HEK293 cells. ★: $p<0.05$ (paired student t test). ★★ : $p < 0.005$ (paired student t test). Error bars represent standard error from three replicates

CHAPTER 4

DISCUSSION

Lamins provide the structural scaffold between the inner nuclear membrane (INM) and chromatin. They also interact directly with chromatin regions involving Lamin associated domains (LADs) (Guelen et al., 2008). The objective of this study was to examine the role of lamins in maintaining chromosomal positioning by perturbing their function through siRNA mediated gene silencing. We also examined transcript levels of candidate genes in lamin depleted cells in order to test the effect of lamins in gene expression profile. Genomic loci FISH was performed to study intrachromosomal dynamics of candidate loci in lamin knock down cells. We utilized biochemical and molecular cytogenetic methods with confocal imaging and image analysis to address potential role of lamins in maintaining chromosomal positioning.

HEK293 cells were preferred as they have two inactive X chromosomes and less karyotypic heterogeneity (Figure 3.6 & 3.7). HEK293 cells were then subjected to siRNA mediated knock down of Lamin A and Lamin B2 followed by immunostaining of Xi markers; H3K27me3 and macro H2A (Figure 3.8). Inactive X chromosome was examined because it is well recognized to display a more peripheral localization (Heard et al., 2005) and lamins could be part of a potential tethering mechanism for Xi chromatin (Figure 1.4). Radial positioning analysis reveals a significant shift in inactive Xi chromosome to a more central position in Lamin B2 depleted cells while no such change is observed in Lamin A depleted cells (Figure 3.10 (a)). This outcome indicates a more prominent role of Lamin B2 compared to Lamin A in maintaining Xi localization. Xi volume shows no difference in Lamin A KD; while Xi volume shows a significant decline in Lamin B2 KD cells. On the other hand Xi surface area is decreased in Lamin A KD nuclei and increase in Lamin B2 KD nuclei (Figure 3.10 (b) & (c)). This discrepancy in Xi territory volume and surface area measurements may be attributed to intrachromosomal topological changes upon lamin depletions. These topological differences could be caused by large scale alteration in epigenetic marks present on Xi. Lamin A mutation is associated with a decrease in epigenetic marks such as H3K27me3 and H3K9me3 and increase in the levels of H4K20me3 on peripheral heterochromatin (Columbaro et al., 2005; Scaffidi and Misteli, 2005; Shumaker et al., 2006). This loss of repressive marks and accumulation of active marks indicates more open chromatin structure and higher transcriptional activity. However, effect of Lamin B2 depletion on heterochromatin remains elusive.

Chromosomal positioning analyses were performed for CTX, CT18 and CT 19 using chromosome specific probes. Radial positioning of CTX show no shift in overall localization of X chromosome territories present in the nucleus (Figure 3.12 (c)). However, inactive X chromosome shows a shift towards the interior of the nucleus in its localization upon Lamin B2 knock down (Figure 3.10 (a)). This discrepancy in radial positioning of CT X and CT Xi could be attributed to the presence of active X

chromosome territory in CT X positioning. Above premise could be tested if one could discriminate active and inactive X chromosomes in the same nuclei. There are two approaches to distinguish active and inactive X chromosomes; first is an ImmunoFISH assay where one can utilize immunostaining against Xi marker proteins like H3K27me3 or macroH2A in combination with 3D FISH assay for X chromosome specific probes. Second approach is to exploit the fact that XIST long non-coding RNA specifically 'coats' the inactive X chromosome by performing an RNA DNA FISH experiment for XIST RNA and CT X specific probes.

Chromosome 18 is a gene poor chromosome and hence demonstrates a peripheral localization in nuclear space. CT18 position is unaltered in Lamin A KD cells but it exhibits a significant shift towards the nuclear periphery in Lamin B2 KD cells (Figure 3.13(a)). This supports our previous prediction that Lamin B2 may have a stronger effect in chromosomal positioning compared to Lamin A. However, CT Xi, showed a more central localization upon Lamin B2 KD; CT 18 shows a more peripheral positioning in Lamin B2 depleted cells. This is contrary to previous reports, which showed a displacement of chromosome 18 from the nuclear periphery to interior in laminopathies (Lamin A mutation) (Mewborn et al., 2007) and MEFs deficient in lamin B1 (Malhas et al., 2007). This suggests a cell type specific role of different lamins in maintaining chromosomal positioning as no difference in CT18 positioning is observed in Lamin A depleted HEK293 cells (Figure 3.13 (a)). Lamin associated domains (LADs) directly interact with lamins and could be both cell type specific (Peric-Hupkes et al., 2010) or conserved (Meuleman et al. 2013). Cell type specific LADs could be possible player in maintaining chromosomal positioning differently across cell types.

CT18 volume remains unaffected in both lamin depleted cells (Figure 3.13 (b)). CT 18 surface area measurements reveal unaltered surface area in Lamin A KD cells but decrease upon Lamin B2 knock down (Figure 3.13(c)). Alteration in surface area while volume remains unchanged is observed again. This could be due to possible architectural or topological changes in chromosome territories upon lamin knock down.

Chromosome 19 is gene rich and demonstrates a more central localization in the nucleus compare to other gene poor chromosomes (Malhas et al., 2007). CT19 does not demonstrate any significant change in its localization upon depletion of either of the lamins (Figure 3.14 (a)). This suggests that the localization of only peripheral chromosomes are affected by lamins as peripherally positioned chromosomes Xi and 18 are affected on Lamin B2 knock down but more centrally located CT19 remains unaltered in terms of its radial positioning. This is consistent with previous findings, which suggests a chromosome specific effect on Lamin A mutant fibroblasts (Mewborn et al., 2010). CT19 volume and surface area is unaffected in Lamin A KD cells but shows a significant decrease in Lamin B2 KD cells (Figure 3.14 (b) & (c)). This alteration in volume and surface area of a centrally located chromosome upon Lamin B2 KD suggests two possibilities: 1. A direct involvement of intranuclear pool

of Lamin B2 in maintaining topological features of chromosome territories. 2. Lamin B2 is indirectly involved upholding the topological features of CTs by some physical or biochemical pathways such as interaction with nuclear matrix (Cau et al., 2014)

qRT PCR experiments were performed to understand the effect of lamin knock downs on expression levels of candidate X chromosome genes. These genes were selected from regions which exhibit X inactivation and PAR regions so as to evaluate differential effect of lamins depletion on transcriptional activity of gene present in these regions. qRT-PCR assays show downregulation of candidate genes that participate in X inactivation but do not affect genes present on PAR regions (Figure 3.17). This suggests a differential mechanism of Lamins exerting its effect on genes present on different chromosomes directly or indirectly. Transcriptional activity may be further correlated with intrachromosomal positioning of these genes based on genomic loci FISH data. *DNMT1* transcript levels were examined because it is directly responsible for maintenance of X chromosome inactivation through DNA methylation (Vasque et al., 2005). Depletion of both Lamin A and Lamin B2 show a comparable decrease in *DNMT1* transcript levels (Figure 3.17). It is possible that a decrease in *DNMT1* would cause a large scale alteration of DNA methylation on Xi and hence affect its transcriptional activity and chromosomal positioning. Bisulfite sequencing could be utilized to examine DNA methylation status of Xi upon lamin depletion.

Genomic loci FISH was performed to investigate dynamics of a genomic loci with respect to chromosome territory in lamin depleted cells. External localization of gene loci (with respect to its chromosome territory) has been demonstrated to correlate with gene overexpression (Christova et al., 2007). Our study suggests that nuclear positioning of *FOXP3* loci does not exhibit any significant shift in Lamin A KD cells but displays a significant decrease in loci present external to X-chromosome territory in Lamin B2 KD cells. We are in process of determining expression levels of FOXP3 upon Lamin A and Lamin B2 KD by qRT PCR. We surmise that decrease in looping out of gene loci would correlate with its transcriptional downregulation. A significant decline has already been demonstrated in expression levels of another X chromosome gene *GNL3L* (Figure 3.17) and this could be more general phenomena in genes participating in X inactivation.

In summary, this study examines the differential roles of Lamins A and B2 in maintaining the positioning of peripheral chromosome 18 and X territories. It also suggests Lamin B2 being a more prominent player in maintaining intranuclear of peripheral chromatin positioning than Lamin A. Large scale topological changes within chromosome territories are shown based on surface area and volume measurements in lamin depleted cells which exhibit significant deviation from untreated cells. Expression levels and localization of candidate genes participating in X inactivation are affected and overall transcriptional profile of Xi could as well be affected since Xi mislocalization is observed in Lamin B2 KD cells. Figure 4.1 is an

overall summary showing the effect of lamin depletion on nuclear topology, chromosome positioning, CT volume and surface area.

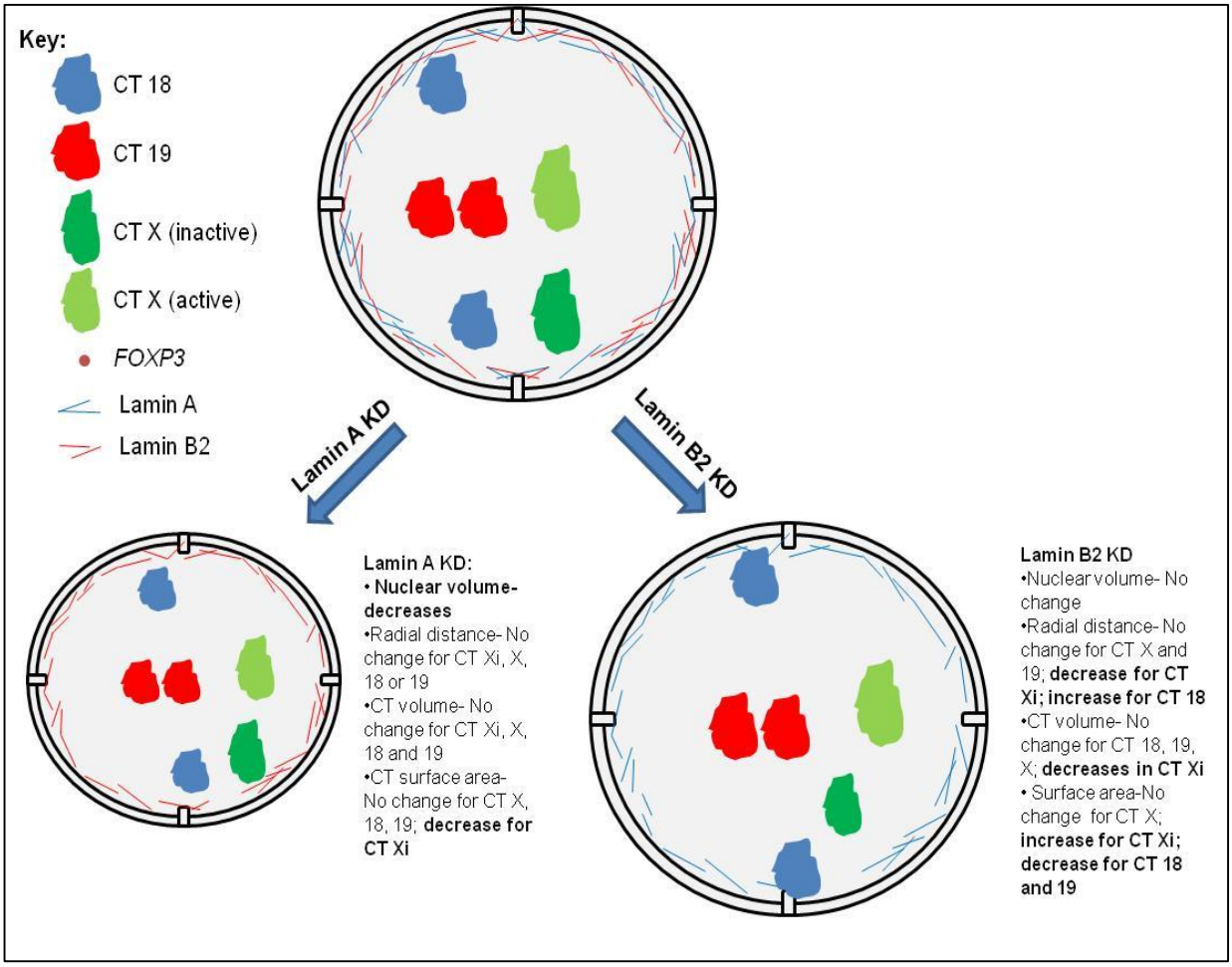

Figure 4.1: Schematic model depicting effect of Lamin A and Lamin B2 KD on nuclear topology, chromosome positioning, CT volume and surface area in HEK293 cells.

References

Barr, M. L. and Bertram, E. G. (1949). A morphological distinction between neurones of the male and female, and the behaviour of the nucleolar satellite during accelerated nucleoprotein synthesis. Nature 163, 676.

Bokenkamp R, Raz V, Venema A, DeRuiter MC, van Munsteren C, Olive M, Nabel EG, Gittenberger- de Groot AC. (2011). Differential temporal and spatial progerin expression during closure of the ductus arteriosus in neonates. PLoS One. 6(9):e23975.

Bolzer A, Kreth G, Solovei I, Koehler D, Saracoglu K, Fauth C, Muller S, Eils R, Cremer C, Speicher MR, et al. (2005). Three- dimensional maps of all chromosomes in human male fibroblast nuclei and prometaphase rosettes. PLoS Biol 3: e157.

Butin-Israeli V, Adam SA, Goldman AE, Goldman RD. (2012). Nuclear lamin functions and disease. Trends Genet. 28(9):464–471.

Calabrese, J.M., Sun, W., Song, L., Mugford, J.W., Williams, L., Yee, D., Starmer, J., Mieczkowski, P., and Crawford, G.E. (2012). Site-specific silencing of regulatory elements as a mechanism of X-inactivation. Cell *151*, 951–963.

Chaumeil, J., Le Baccon, P., Wutz, A. and Heard, E. (2006). A novel role for Xist RNA in the formation of a repressive nuclear compartment into which genes are recruited when silenced. Genes Dev. 20, 2223-2237.

Christova, R., Jones, T., Wu, P.J., Bolzer, A., Costa-Pereira, A.P., Watling, D., Kerr, I.M., and Sheer, D. (2007). P-STAT1 mediates higher-order chromatin remodelling of the human MHC in response to IFNgamma. J Cell Sci *120*, 3262-3270.

Clemson, C.M., Hall, L.L., Byron, M., McNeil, J., and Lawrence, J.B. (2006). The X chromosome is organized into a gene-rich outer rim and an internal core containing silenced nongenic sequences. Proceedings of the National Academy of Sciences of the United States of America *103*, 7688–7693.

Coffinier C, Jung HJ, Nobumori C, Chang S, Tu Y, Barnes RH 2nd, Yoshinaga Y, de Jong PJ, Vergnes L, Reue K, Fong LG, Young SG. (2011). Deficiencies in lamin B1

and lamin B2 cause neurodevelopmental defects and distinct nuclear shape abnormalities in neurons. Mol Biol. Cell. 22: 4683-93.

Columbaro M, Capanni C, Mattioli E, Novelli G, Parnaik VK, Squarzoni S, Maraldi NM, Lattanzi G. (2005). Rescue of heterochromatin organization in Hutchinson-Gilford progeria by drug treatment. 62: 2669–78.

Croft JA, Bridger JM, Boyle S, Perry P, Teague P, et al. (1999) Differences in the localization and morphology of chromosomes in the human nucleus. J Cell Biol 145: 1119–1131.

Croft, J.A., J.M. Bridger, S. Boyle, P. Perry, P. Teague, and W.A. Bickmore. (1999). Differences in the localization and morphology of chromosomes in the human nucleus. J. Cell Biol. 145:1119–1131.

Dechat T, Adam SA, Taimen P, Shimi T, Goldman RD. (2010). Nuclear lamins. Cold Spring Harb Perspect Biol 2: a000547.

Dechat, T., Pfleghaar, K., Sengupta, K., Shimi, T., Shumaker, D.K., Solimando, L., and Goldman, R.D. (2008). Nuclear lam- ins: Major factors in the structural organization and function of the nucleus and chromatin. Genes & Dev. 22: 832–853.

Dittmer TA, Misteli T. (2011). The lamin protein family. Genome Biol 12: 222.

Elizabeth A. Booth-Gauthier , Vicard Du , Marion Ghibaudo , Andrew D. Rape , Kris Noel Dahl and Benoit Ladoux.(2013). Hutchinson–Gilford progeria syndrome alters nuclear shape and reduces cell motility in three dimensional model substrates. Integr. Biol. 5, 569-577.

Engel E. (1980). A new genetic concept: uniparental disomy and its potential effect, isodisomy. Am J Med Genet*;* 6*:* 137–43.

Gendrel, A.-V., and Heard, E. (2011). Fifty years of X-inactivation research. Development (Cambridge, England) *138*, 5049–5055.

Graham FL, Smiley J, Russell WC, Nairn R. (1977). Characteristics of a human cell line transformed by DNA from human adenovirus type 5. J. Gen. Virol. 36 (1): 59–74.

Guelen L, Pagie L, Brasset E, Meuleman W, Faza MB, Talhout W, Eussen BH, de Klein A, Wessels L, de Laat W, van Steensel B. (2008) Domain organization of human chromosomes revealed by mapping of nuclear lamina interactions. Nature. 453(7197):948–951.

Håkelien, A.-M., Delbarre, E., Gaustad, K.G., Buendia, B., and Collas, P. (2008). Expression of the myodystrophic R453W mutation of lamin A in C2C12 myoblasts causes promoter-specific and global epigenetic defects. Experimental Cell Research *314*, 1869–1880.

Heard, E. (2005). Delving into the diversity of facultative heterochromatin: the epigenetics of the inactive X chromosome. Current Opinion in Genetics & Development *15*, 482–489.

Leibovitz, A., Stinson, J.C., Iii, W.B.M., Leibovltz, A., Stlnson, J.C., Mccombs, W.B., and Mabry, N.D. (1976). Classification of Human Colorectal Adenocarcinoma Cell Lines Classification of Human Colorectal Adenocarcinoma Cell Lines. 4562–4569.

Lieberman-Aiden, E., Van Berkum, N.L., Williams, L., Imakaev, M., Ragoczy, T., Telling, A., Amit, I., Lajoie, B.R., Sabo, P.J., Dorschner, M.O., et al. (2009). Comprehensive mapping of long-range interactions reveals folding principles of the human genome. Science (New York, N.Y.) *326*, 289–293.

Malhas, A., Lee, C.F., Sanders, R., Saunders, N.J., and Vaux, D.J. (2007). Defects in lamin B1 expression or processing affect interphase chromosome position and gene expression. J. Cell Biol. 176: 593–603.

Matarazzo, M.R., Boyle, S., Esposito, M.D., and Bickmore, W.A. (2007). Chromosome territory reorganization in a human disease with altered DNA methylation. PNAS *104*, 16536–16551.

Melcer, S., Gruenbaum, Y., and Krohne, G. (2007). Invertebrate lamins. Exp Cell Res *313*, 2157-2166.

Melcher R, Steinlein C, Feichtinger W, Müller CR, Menzel T, Lührs H, Scheppach W, Schmid M. (2000). Spectral karyotyping of the human colon cancer cell lines SW480 and SW620. Cytogenet Cell Genet., 88, 145-52.

MeulemanW, Peric-HupkesD, Kind J, Beaudry JB, Pagie L, Kellis M, Reinders M, Wessels L, van Steensel B. (2013). Constitutive nuclear lamina– genome interactions are highly conserved and associated with A/T-rich sequence. Genome Res 23: 270–280.

Mewborn, S.K., Puckelwartz, M.J., Abuisneineh, F., Fahrenbach, J.P., Zhang, Y., MacLeod, H., Dellefave, L., Pytel, P., Selig, S., Labno, C.M. (2010). Altered chromosomal positioning, compaction, and gene expression with a lamin A/C gene mutation. PloS One *5*, e14342.

Peric-Hupkes D, Meuleman W, Pagie L, Bruggeman SWM, Solovei I, Brugman W, Gra¨ f S, Flicek P, Kerkhoven RM, Van Lohuizen M, et al. 2010. Molecular maps of the reorganization of genome–nuclear lamina interactions during differentiation. Mol Cell 38: 603–613.

Prokocimer, M., Davidovich, M., Nissim-Rafinia, M., Wiesel-Motiuk, N., Bar, D.Z., Barkan, R., Meshorer, E., and Gruenbaum, Y. (2009). Nuclear lamins: key regulators of nuclear structure and activities. Journal of Cellular and Molecular Medicine *13*, 1059–1085.

Schumacher, J., Reichenzeller, M., Kempf, T., Schnolzer, M., and Herrmann, H. (2006). Identification of a novel, highly variable amino-terminal amino acid sequence element in the nuclear intermediate filament protein lamin B(2) from higher vertebrates. FEBS Lett. 580: 6211–6216.

Shah, P.P., Donahue, G., Otte, G.L., Capell, B.C., Nelson, D.M., Cao, K., Aggarwala, V., Cruickshanks, H. a, Rai, T.S., McBryan, T., et al. (2013). Lamin B1 depletion in senescent cells triggers large-scale changes in gene expression and the chromatin landscape. Genes & Development *27*, 1787–1799.

Shumaker, D.K., Dechat, T., Kohlmaier, A., Adam, S.A., Bozovsky, M.R., Erdos, M.R., Eriksson, M., Goldman, A.E., Khuon, S., Collins, F.S., et al. (2006). Mutant nuclear lamin A leads to progressive alterations of epigenetic control in premature aging. *21*, 21–26.

Simon DN, Wilson KL. (2011). The nucleoskeleton as a genome-associated dynamic ‘network of networks’. Nat Rev Mol Cell Biol. 12(11):695–708.

Simonis M, Klous P, Splinter E, Moshkin Y, Willemsen R, de Wit E, van Steensel B, de Laat W. (2006). Nuclear organization of active and inactive chromatin domains

uncovered by chro- mosome conformation capture-on-chip (4C). Nat Genet 38: 1348–1354.

Solovei, I., Wang, A.S., Thanisch, K., Schmidt, C.S., Krebs, S., Zwerger, M., Cohen, T. V, Devys, D., Foisner, R., Peichl, L., et al. (2013). LBR and lamin A/C sequentially tether peripheral heterochromatin and inversely regulate differentiation. Cell *152*, 584–598.

Vasques, L.R., Stabellini, R., Xue, F., Tian, X.C., and Soukoyan, M. (2006). XIST Repression in the Absence of DNMT1 and DNMT3B. *378*, 373–378.

Winnard P Jr, Glackin C, Raman V. (2006). Stable integration of an empty vector in MCF-7 cells greatly alters the karyotype. Cancer Genet Cytogenet. ,164(2):174-6.

Worman HJ. (2012). Nuclear lamins and laminopathies. J Pathol. 226(2):316–325.

Wutz, A. (2011). Gene silencing in X-chromosome inactivation : advances in understanding facultative heterochromatin formation. Nature Publishing Group 12, 542–553.